

Downstream variations of air-gap membrane distillation and comparative study with direct contact membrane distillation: A modelling approach

Author

Ansari, Abolfazl, Galogahi, Fariba Malekpour, Thiel, David, Helfer, Fernanda, Millar, Graeme, Soukane, Sofiane, Ghaffour, Noreddine

Published

2022

Journal Title

Desalination

Version

Accepted Manuscript (AM)

DOI

[10.1016/j.desal.2021.115539](https://doi.org/10.1016/j.desal.2021.115539)

Rights statement

© 2022 Elsevier. Licensed under the Creative Commons Attribution-NonCommercial-NoDerivatives 4.0 International Licence (<http://creativecommons.org/licenses/by-nc-nd/4.0/>) which permits unrestricted, non-commercial use, distribution and reproduction in any medium, providing that the work is properly cited.

Downloaded from

<http://hdl.handle.net/10072/417225>

Griffith Research Online

<https://research-repository.griffith.edu.au>

Downstream Variations of Air-Gap Membrane Distillation and Comparative Study with Direct Contact Membrane Distillation: A Modelling Approach

Abolfazl Ansari ^{a,*}, Fariba Malekpour Galogahi ^a, David V Thiel ^a, Fernanda Helfer ^a, Graeme Millar ^b, Sofiane Soukane ^c, Noredine Ghaffour ^c

^a School of Engineering and Built Environment, Griffith University, Brisbane, QLD 4111, Australia

^b Institute for Future Environments, School of Mechanical, Medical & Process Engineering, Science and Engineering Faculty, Queensland University of Technology (QUT), Brisbane, Queensland 4000, Australia

^c King Abdullah University of Science and Technology (KAUST), Water Desalination and Reuse Center (WDRC), Biological and Environmental Science & Engineering (BESE) Division, Thuwal 23955-6900, Saudi Arabia

* Corresponding author at: School of Engineering and Built Environment, Griffith University, Brisbane, QLD 4111, Australia. E-mail address: abolfazl.ansari@griffithuni.edu.au (A. Ansari)

Abstract

Air-Gap Membrane Distillation (AGMD) promises to reduce heat loss in membrane distillation. Most AGMD models are one-dimensional and do not consider the downstream variations. In addition, a linear function of vapour pressure is used, which either relies on experimentally determined parameters or a simplified mass transfer resistance to model the water permeate flux. This study introduces a new, improved model that simultaneously considers both heat and mass transfer in the AGMD process by coupling the continuity, momentum, and energy equations. A novel precise logarithmic function of vapour pressure was derived to model the water permeate flux, independent of experimentally determined parameters. By varying the inlet temperature, Reynolds number, inlet concentration, and air-gap thickness, the performance of AGMD was evaluated. The results revealed that our model improved the water flux prediction from more than 10% to less than 4% deviation from experimental results. Among the operating conditions, only increasing the Reynolds number improved all the system performance metrics, including higher water flux and lower temperature and concentration polarisation effects. Results were compared with Direct Contact Membrane Distillation (DCMD) outcomes and showed that unlike AGMD, DCMD suffers from a substantial decrease in water flux along the module. For DCMD, the exit water flux value decreased by 50% in comparison with the inlet value, while the water flux decreased by only 2% for AGMD, using a 1mm air gap thickness.

Keywords: Direct Contact Membrane Distillation; Air-Gap Membrane Distillation; Modelling; Temperature Polarisation, Concentration Polarisation

51 efficiency compared to the leading thermal process, such as multi-effect distillation.
52 Therefore, detailed sensitivity analysis of various parameters on the MD process throughout
53 the module provides an essential insight into the MD process and MD membrane fabrication
54 [3, 5, 6].

55 Mathematical modelling enables us to predict and analyse the influence of significant
56 parameters such as operating conditions on MD performance. To date, considerable research
57 has been conducted on MD modelling, most of which focused on the Direct Contact
58 Membrane Distillation (DCMD) technique [3, 7-11]. Air Gap Membrane Distillation (AGMD) as
59 a method to reduce the heat loss and enhance the MD thermal efficiency needs to be
60 meticulously modelled, analysed, and improved [12-19]. Alssadi et al. [13, 14] developed a 1-
61 D mathematical model for a flat sheet AGMD module, running under atmospheric and sub-
62 atmospheric conditions. The essential parameters to scale up an AGMD system and the effect
63 of removing non-condensable gases from an AGMD module were investigated. The model
64 predicted the water vapour flux within a 10% error. Computational Fluid Dynamics (CFD) has
65 been widely used to implement numerical modelling on MD [9]. Alklaibi et al. [20] carried out
66 a CFD simulation study to provide sensitivity analysis for a AGMD configuration. However, a
67 simple correlation for the transmembrane water flux was applied and no information about
68 the solute concentration along the module was provided. Karbasi et al. [21] conducted a 3-D
69 numerical simulation on a novel disc-type module in the AGMD system and compared the
70 results with the rectangular-type module. However, some simple assumptions were made to
71 model the water flux across the membrane. In addition, parametric study and temperature
72 and concentration polarisation effects were not discussed. Due to the complexity of the
73 multiphase model of water vapour across the air gap, to the best of our knowledge, all
74 previously published CFD studies have been based on many simple assumptions to simulate
75 the AGMD technique [22]. In addition, CFD is a high-complexity and time-consuming
76 approach; therefore, what makes CFD more valuable and justifiable for use in AGMD is the
77 investigation of condensation in the air gap and the study of variations in flow properties
78 throughout the module. In our study, a new, improved mathematical model uses the CFD and
79 heat and mass transfer model, calculated using Nusselt and Sherwood Correlation, to benefit
80 from both CFD and the less time-consuming approach of the Nusselt and Sherwood
81 Correlation model.

82 Energy efficiency is one of the main challenges that should be addressed, to make MD cost-
83 effective. MD suffers from significant downstream variations of heat transfer along the MD
84 module, leading to low energy efficiency. The air gap was introduced to make the flow
85 temperature more uniform and to decrease the heat loss in MD system [23-25]. To the best
86 of our knowledge, no modelling study on AGMD has reported the downstream variations of
87 flow properties throughout the AGMD module. Most studies have made assumptions, such
88 as constant feed and permeate temperatures along the module. In this study, we investigated
89 the downstream variations of temperature along the module to provide the transmembrane
90 water flux, Temperature Polarisation Coefficient (TPC), Concentration Polarisation Coefficient
91 (CPC), and thermal efficiency. The results of downstream variations are essential to evaluate
92 the importance of introducing direct solar heating as a promising method to localise the
93 temperature distribution along the MD module [26-28].

94 In MD modelling, the transmembrane water flux is crucial because it affects all the other flow
95 properties throughout the module. Most MD modelling studies rely on constant fitting
96 parameters, which are determined from a specific set of experimental conditions. Of the
97 studies that have included a formula to model the water flux transmembrane, a simplified
98 form of Dusty Gas Model (DGM) has been investigated. Indeed, both membrane and air gap
99 have not been integrated to derive a more precise model [29]. Noamani et al. [12] introduced
100 a model that used a linear function of water vapour pressure and total mass transfer to model
101 the water flux; however, they did not integrate over both membrane and air gap of the AGMD
102 system. Khalife et al. [30] used a simplified model to investigate the effect of different
103 operating parameters on permeate water flux. Moreover, in MD the air is assumed to move
104 counter to the water flux; so that an improved model will include the effect of air flux on the
105 water flux. In this study, a detailed transmembrane water flux model, which includes three
106 diffusive mass transfer mechanisms and with consideration of the counter-air flux, is
107 presented.

108 Temperature and concentration polarisation are two main negative phenomena that need to
109 be investigated throughout the module [31]. In the literature, there is limited discussion on
110 the spread of solute concentration along the AGMD module [32-34]. Extensive experiments
111 have been conducted to evaluate the effect of membrane properties on the AGMD
112 performance [35-38]. In our study, different commercial membranes were critically compared
113 in terms of different membrane properties. Finally, few AGMD studies have numerically and
114 critically compared DCMD and AGMD in terms of downstream variations of flow properties
115 [39, 40].

116 Although the existing models provide many advantages for MD process modelling, there are
117 still some critical concerns to be investigated. This study aims to present an improved model
118 to capture the downstream variation throughout the AGMD module, and to carry out a
119 comprehensive and comparative study on AGMD and DCMD performance. The improved
120 model predicts transmembrane water flux, TPC, CPC, and thermal efficiency, by using a new
121 transmembrane model that benefits from two advantages. First, it is independent of any
122 other determined parameters from a specific experiment, which enables the analysis of
123 membrane properties and commercially available membranes. Second, it includes both a flux
124 derived from the diffusion applied on the bulk fluid and a flux derived from the bulk motion
125 on the fluid.

126 Within the above context the following specific objectives were set for this study:

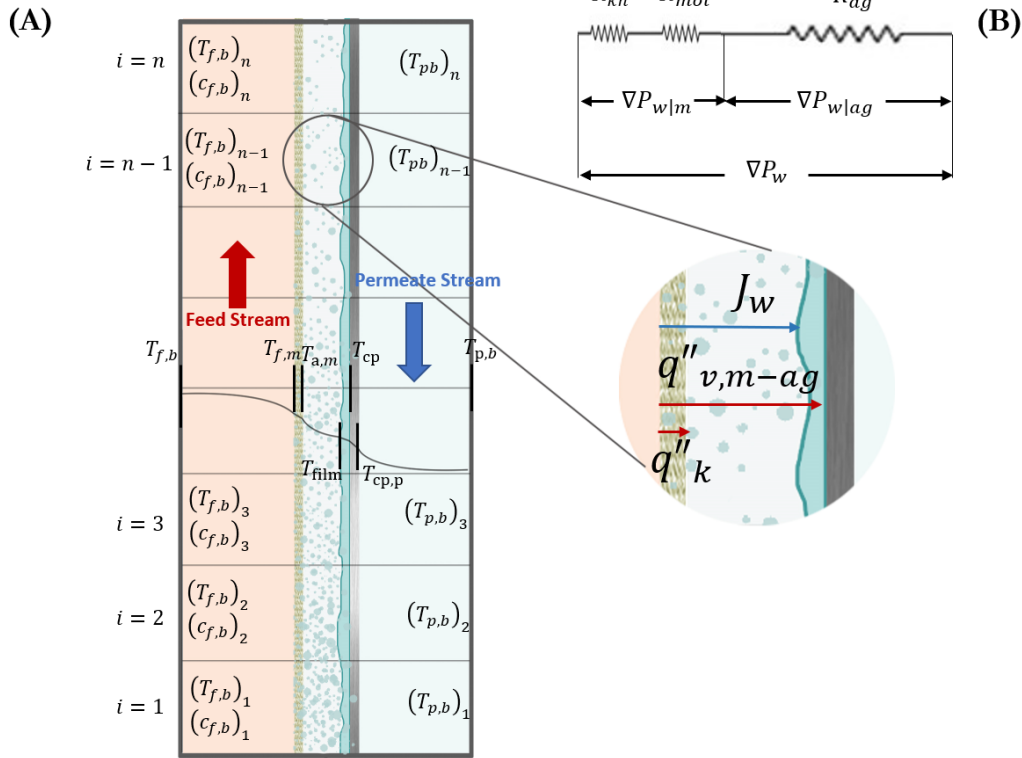
- 127 1. To develop a model that can capture the downstream variation of water flux of an
128 AGMD system.
- 129 2. To formulate a self-sustained water flux equation, which is the most significant
130 parameter in AGMD modelling studies, with the least assumptions.
- 131 3. To implement a parametric study analysis to understand which parameters
132 significantly impact AGMD performance.
- 133 4. To conduct a comparison study of AGMD with DCMD, including downstream
134 variations and systems performance metrics.

135 In this study, a novel computational model is developed by contributing a new water flux
136 model and by employing continuity, momentum, and energy equations to capture
137 downstream variations and analyse AGMD performance. The modelling procedure and
138 influence of each parameter on AGMD performance including water flux permeation, thermal
139 efficiency, TPC, and CPC are provided in detail, and a comparative study of AGMD and DCMD
140 at similar conditions is also presented.

141 **2. Materials and Methods**

142 **2.1. Governing Equation**

143 A theoretical model that considers both heat and mass transfer was improved for the AGMD
144 system. A 2-D, counter-current, flat-sheet AGMD module with feed, air, and permeate
145 channels was modelled, as shown in Figure 1. A saline water with velocity V_{in} , temperature
146 $T_{f,b}$, and concentration C_{in} enters the feed channel, and pure water with velocity V_{in} and
147 temperature $T_{p,b}$ enters the permeate channel in the counter direction of feed flow. As the
148 feed flows through the module, evaporation takes place and produces vapour, which moves
149 across the hydrophobic membrane pores. Subsequently, the vapour diffuses through the
150 stagnant air that is introduced between the membrane and condensing plate. As shown in
151 Figure 2, AGMD occurs in six stages: feed channel, membrane, air channel, condensate film,
152 cooling plate, and permeate channel. The process happening in each stage results in a
153 resistance to heat and mass transfer. The assumptions for heat and mass transfer modelling
154 include: a steady state condition; uniform total pressure (1 atm); negligible viscous flow, slip
155 flow surface diffusion, and pressure diffusion; stagnant air within air channel (and therefore
156 no counter air movement against the water flux); no heat loss from the system to the
157 environment; negligible convection heat transfer in the air-gap channel,; laminar flow for the
158 liquid film; negligible shear stress at the liquid-vapor interface; and negligible momentum and
159 energy transfer by advection in the condensate film.



160

161 **Figure 1.** (A) Elements used to study the downstream properties of an AGMD module. ‘ T ’, ‘ c ’, ‘ J ’, and
 162 ‘ q'' ’ represent the temperature, salt concentration, flux, and heat transfer flux, respectively. Subscripts
 163 ‘ f ’, ‘ p ’, ‘ w ’, ‘ v ’, ‘ k ’ refer to the feed, permeate sides, water vapour, vapour latent heat, and conduction
 164 heat transfer, respectively, and ‘ b ’, ‘ m ’, and ‘ $m-ag$ ’ refer to bulk, membrane, and membrane plus air
 165 gap locations in the module. (B) Mass transfer resistance model in AGMD process. ‘ R ’ and ‘ ∇P ’
 166 represent mass resistance and pressure difference, respectively. Subscripts ‘ Kn ’, ‘ mol ’, ‘ w ’, ‘ m ’ and ‘ ag ’
 167 refer to Knudsen, molecular, water vapour, membrane and air-gap, respectively.

168 2.1.1. Heat Transfer

169 Figure 2. shows the thermal resistance in the AGMD process. Heat transfer occurs from the
 170 hot side to the cool side. By solving the steady-state energy balance equations, the
 171 temperatures at different locations along the module, including $T_{f,m}$ and T_{film} , can be
 172 obtained as follows:

$$Q''_f = Q''_{m+ag} = Q''_{film} = Q''_{cp} = Q''_p \quad (1)$$

$$h_f(T_{f,b} - T_{f,m}) = h_{am}(T_{f,m} - T_{film}) + (J_w)_{m-ag}h_{fg} = h_{film}(T_{film} - T_{cp}) = h_{cp}(T_{cp} - T_{cp,p}) = h_p(T_{cp,p} - T_{p,b}) \quad (2)$$

$$T_{f,m} = T_{f,b} - \frac{h_T}{h_f} \left((T_{f,b} - T_{p,b}) + \frac{(J_w)_{m-ag}h_{fg}}{h_{am}} \right) \quad (3)$$

$$T_{film} = T_{p,b} + \frac{h_T}{h_{f,cp,p}} \left((T_{f,b} - T_{p,b}) + \frac{(J_w)_{m-ag}h_{fg}}{h_{am}} \right) \quad (4)$$

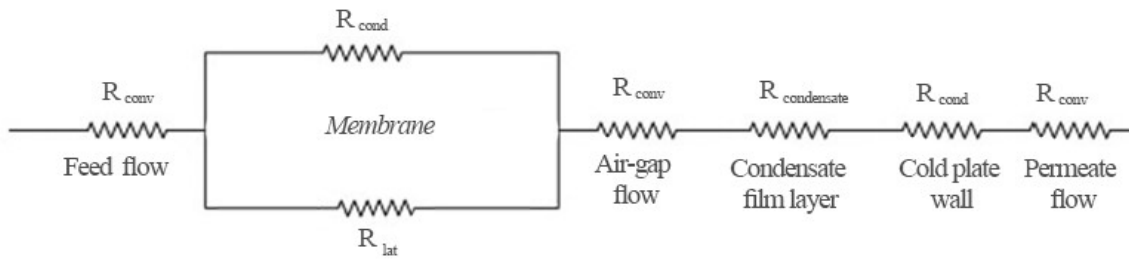
$$h_T = \left(\frac{1}{h_f} + \frac{1}{h_{am}} + \frac{1}{h_{f,cp,p}} \right)^{-1} \quad (5)$$

$$h_{f,cp,p} = \left(\frac{1}{h_{film}} + \frac{1}{h_{cp}} + \frac{1}{h_p} \right)^{-1} \quad (6)$$

173

174 where Q''_f is the heat flux from the feed bulk to the membrane surface, Q''_{m+ag} is the heat
 175 flux transferred through the membrane and air gap channel, Q''_{film} is the heat flux across the
 176 condensation film, Q''_{cp} is the heat flux across the cooling plate, Q''_p is the heat flux from the
 177 cooling plate to the permeate bulk, h_f is the convective heat transfer of the feed, $T_{f,b}$ is the
 178 bulk feed temperature, $T_{cp,p}$ is the cold plate temperature at the permeate side, $T_{p,b}$ is the
 179 bulk permeate temperature, h_p is the convective heat transfer of the permeate, h_T is the
 180 overall heat transfer coefficient of the system, and $h_{f,cp,p}$ is the overall heat transfer
 181 coefficient from the condensate film to the permeate side.

182



183

184 **Figure 2.** Electrical analogy of heat transfer resistance in AGMD. Due to temperature difference, heat
 185 passes from the feed side to permeate side. The heat transfer is the same through each stage of the
 186 process, namely: feed-side, membrane, air-gap, condensate layer, cold plate and permeate side. Heat
 187 transfer throughout the membrane includes the latent heat of evaporation and conduction heat
 188 transfer.

189 2.1.1.1. Channel Flow

190 The feed and permeate heat transfer coefficient can be obtained by using dimensionless
 191 Nusselt number to estimate the feed and permeate heat transfer across the module,
 192 Equations (A1-A4) (Appendix A). Although density, viscosity, specific heat transfer, and mass
 193 diffusivity do not change significantly along the module, all the properties throughout the
 194 module are updated using Equations (A5-A8).

195 2.1.1.2. Transmembrane and Air Gap Channel

196 The heat conduction transfer through the membrane and the latent heat transfer owing to
 197 the flux of water vapour across the membrane and air gap both contribute to heat transfer
 198 across the membrane, shown in Figure 1.

$$q''_{k,m} = h_m(T_{f,m} - T_{am}) \quad (7)$$

$$h_m = \frac{k_e}{\delta} \quad (8)$$

$$q''_{fg} = (J_w)_{m-ag} h_{fg} \quad (9)$$

199 where $q''_{k,m}$ is the transmembrane conductive heat transfer flux, h_m is the membrane heat
 200 transfer coefficient, $T_{f,m}$ is the membrane feed side temperature, T_{am} is the membrane
 201 permeate side temperature, k_e is the effective thermal conductivity of membrane, δ is the
 202 membrane thickness, and h_{fg} is the latent heat.

203 Since natural convection in the air gap is negligible [20], in our study, only conduction heat
 204 transfer was assumed as Equation (10).

$$h_a = \frac{k_a}{b} \quad (10)$$

$$h_{am} = \frac{1}{\frac{1}{h_m} + \frac{1}{h_a}} \quad (11)$$

205 where k_a , b , h_a and h_{am} are thermal conductivity of air, air gap thickness, air heat transfer
 206 coefficient, and coupled air and membrane heat transfer coefficient, respectively.

207 2.1.1.3. The Condensate Film and Cooling Plate

208 As shown in Figure 2, the condensation film formed by condensing water vapour, transfers
 209 heat via conduction and convection. The value of convective heat transfer compared to
 210 conduction heat transfer is negligible because the ratio of conductive to convective heat
 211 transfer is a function of a second power of the condensate film thickness, which is negligible
 212 [41]. Heat transfer then occurs through the cooling plate. Therefore, the film heat transfer
 213 coefficient and the plate heat transfer coefficient can be calculated by Equations (12-13) [41].

$$h_{film} = 0.943 \left[\frac{\rho^2 g h_{fg} k_{t,K,p}^3}{\mu L (T_{sat,1atm} - T_{cp})} \right]^{0.25} \quad (12)$$

$$h_{cp} = \frac{k_{cp}}{\delta_{cp}} \quad (13)$$

214 where h_{film} is the convective heat transfer coefficient of film layer, ρ is the density of water,
 215 g is the gravitational acceleration, h_{fg} is the latent heat of evaporation, k is the thermal
 216 conductivity, μ is the viscosity, L is the length of cooling plate, T_{film} , and T_{cp} are
 217 temperatures of film, and cooling plate, respectively. k_{cp} , δ_{cp} , and h_{cp} are thermal
 218 conductivity, cooling plate thickness, and heat transfer coefficient of the plate, respectively.

219 2.1.2. Mass Transfer

220 The Dusty Gas Model (DGM) is a transport model used to simulate the motion of fluid
 221 mixtures through a porous media. When isothermal conditions are assumed, the gradients of
 222 pressure, concentration, and partial pressure lead to viscous flow, ordinary diffusion, and
 223 Knudsen flow [42]. Slip flow, pressure diffusion, and surface diffusion can be disregarded and
 224 because total pressure remains constant at 1 atm and , the viscous flow is also theoretically
 225 neglected [42]. In MD, the water flux through the membrane can be described through three
 226 mechanisms: Knudsen diffusion, molecular diffusion, and a combination of Knudsen and
 227 molecular diffusion. The Knudsen number, used to define the type of mechanism, can be
 228 defined as the ratio of the mean free path of the gas to the pore diameter, as shown in
 229 Equations (A9-A10) [43]. In this section, the water flux passed through both the membrane
 230 and air gap was calculated. The serial connection of membrane and air-gap resistances, shown
 231 in Figure 1 (B), allowed writing the expression below as Equation (14). Equations (15) and (16)
 232 were derived using Fick's law and Graham's law [41, 44] then by substituting Equations (15)
 233 and (16) into Equation (14), the expression for water permeation flux was obtained as
 234 Equation (17). Integration of Equation (18) provided the steady-state water vapour flux for
 235 the transition region ($0.01 < kn < 1$) in the AGMD process (Equation (19)). The water flux
 236 for the case of Knudsen ($kn > 1$) and molecular diffusion ($kn < 0.01$) are also provided as
 237 Equations (A15) and (A14), respectively in Appendix (A) [42, 44].

$$\frac{\nabla P_{w|m-ag}}{(J_w)_{m-ag}} = \frac{\nabla P_{w|m}}{(J_w)_m} + \frac{\nabla P_{w|ag}}{(J_w)_{ag}} \quad (14)$$

$$(J_w)_m = -\frac{M_w}{RT_m \delta} \left(\frac{P_t - (1 - \alpha_1)P_w}{(\epsilon/\tau)(P_t D_{v-a})_m} + \frac{1}{D_{kn}} \right)^{-1} \nabla P_{w|m} \quad [42](15)$$

$$(J_w)_{ag} = -\frac{M_w}{RT_{ag} b} \left(\frac{P_t - (1 - \alpha_2)P_w}{(P_t D_{v-a})_{ag}} \right)^{-1} \nabla P_{w|ag} \quad (16)$$

$$\frac{\nabla P_{w|m-ag}}{(J_w)_{m-ag}} = -\frac{RT_m \delta}{M_w} \left(\frac{P_t - (1 - \alpha_1)P_w}{(\epsilon/\tau)(P_t D_{v-a})_m} + \frac{1}{D_{kn}} \right) - \frac{RT_{ag} b}{M_w} \left(\frac{P_t - (1 - \alpha_2)P_w}{(P_t D_{v-a})_{ag}} \right) \quad (17)$$

$$(J_w)_{m-ag} = -\frac{M_w}{R} \left(T_m \delta \left(\frac{P_t - (1 - \alpha_1)P_w}{(\epsilon/\tau)(P_t D_{v-a})_m} + \frac{1}{D_{kn}} \right) + T_{ag} b \left(\frac{P_t - (1 - \alpha_2)P_w}{(P_t D_{v-a})_{ag}} \right) \right)^{-1} \nabla P_{w|m-ag} \quad (18)$$

$$(J_w)_{m-ag} = \frac{M_w (\epsilon/\tau) (P_t D_{v-a})_m (P_t D_{v-a})_{ag}}{R [\delta (1 - \alpha_1) T_m (P_t D_{v-a})_{ag} + b (\epsilon/\tau) (1 - \alpha_2) T_{ag} (P_t D_{v-a})_m]} \quad (19)$$

$$\ln \left[\frac{D_{kn} [T_m \delta (P_t D_{v-a})_{ag} (P_t - (1 - \alpha_1) P_{v, film}) + T_{ag} b (P_t D_{v-a})_m (\epsilon/\tau) (P_t - (1 - \alpha_2) P_{v, film})] + T_m \delta (\epsilon/\tau) (P_t D_{v-a})_m (P_t D_{v-a})_{ag}}{D_{kn} [T_m \delta (P_t D_{v-a})_{ag} (P_t - (1 - \alpha_1) P_{v, fm}) + T_{ag} b (P_t D_{v-a})_m (\epsilon/\tau) (P_t - (1 - \alpha_2) P_{v, fm})] + T_m \delta (\epsilon/\tau) (P_t D_{v-a})_m (P_t D_{v-a})_{ag}} \right]$$

238 where P is the vapour pressure, J is the permeate flux of water through, M_w is the molecular
 239 weight of water, M_a is the molecular weight of air, α_1 is the effect of air flux in membrane,
 240 α_2 is the effect of air flux in the air-gap channel, which is equal zero for the case of a
 241 diffusion through stagnant air, R is the universal gas constant, ϵ is the membrane porosity,
 242 d_p is the membrane pore diameter, δ is the membrane thickness, b is the air gap channel
 243 thickness, τ is the membrane tortuosity, P_t is the total pressure in the membrane pores, D_{kn}
 244 is the Knudsen diffusion coefficient, D_{v-a} is the water–vapour diffusivity in the air, T is the

245 average temperature, $p_{v,fm}$ is the water vapour pressure on the feed side of membrane,
 246 $p_{v,am}$ is the water vapour pressure on the air side of membrane, and $p_{v,film}$ is the water
 247 vapour pressure on the condensate film. The subscripts $m - ag, ag, m,$ and t refer to
 248 membrane plus air gap, air gap, membrane, and transition region, respectively.

249 2.2. Process Modelling

250 As shown in Figure 1, the feed, air, and permeate channels were divided into n elements, and
 251 the continuity, Navier-Stokes, and energy equations were solved by employing Fluent ANSYS.
 252 As the heat along the feed channel transferred to the permeate side, the bulk feed
 253 temperature along the membrane decreased, whereas the permeate temperature increased.
 254 The obtained bulk temperatures enabled calculation of flow properties across the module,
 255 membrane temperatures on both sides, and condensate film temperature. The equations to
 256 compute membrane temperature on both sides and condensate film in the semi-empirical
 257 model were dependent on water flux. Therefore, the effects of water flux on the temperature
 258 results on the numerical model were included, and the algorithm illustrated in Figure 3 was
 259 applied to couple the temperature results of numerical simulation with the empirical model
 260 for each element.

261 The governing equations of numerical simulation in the feed, air, and permeate channel flow
 262 are the continuity, Navier-Stokes, and energy equations [45], as follows: We used the results
 263 from the numerical simulation as an initial input for the algorithm illustrated in Figure 3.

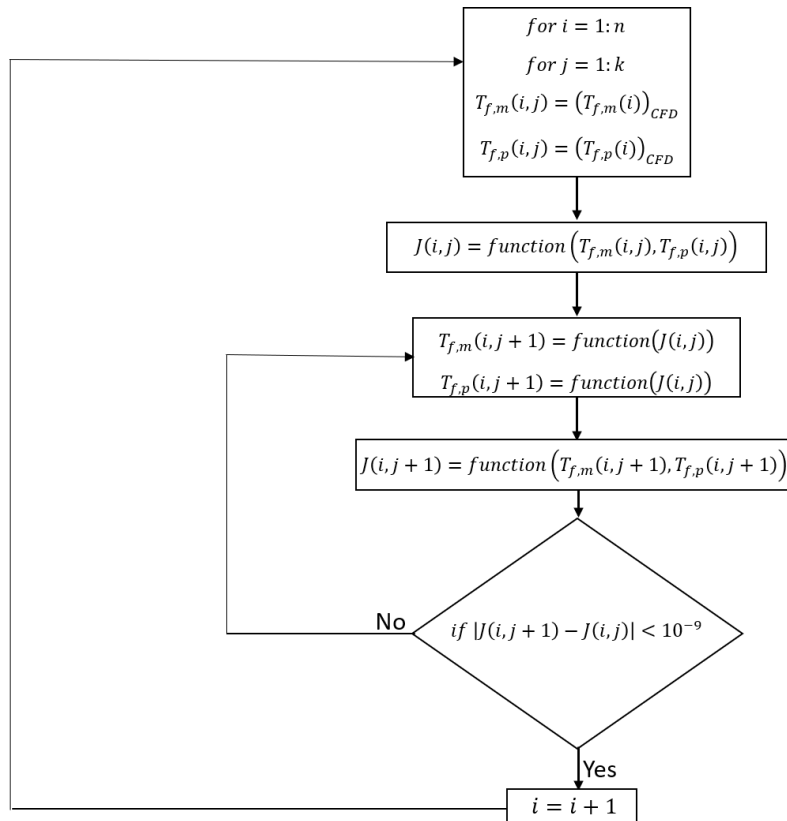
$$\nabla \cdot \vec{V} = 0 \quad (20)$$

$$\rho \left[\frac{\partial \vec{V}}{\partial t} + (\vec{V} \cdot \nabla) \vec{V} \right] = -\nabla p + \mu \nabla^2 \vec{V} + \rho g \quad (21)$$

$$\frac{\partial T}{\partial t} + (\vec{V} \cdot \nabla) T = \frac{k_f}{\rho c_p} \nabla^2 T \quad (22)$$

264 where $\vec{V} = [u \ v]$ is the fluid velocity vector, T is the temperature, p is the pressure, μ is the
 265 viscosity, k_f is the thermal conductivity, c_p is the fluid heat capacity, ρ is the mixture density,
 266 and g is the gravity acceleration.

267 The pressure-based method, the SIMPLE algorithm, and a second-order accuracy for the
 268 spatial discretisation scheme were employed to solve the steady-state governing equations
 269 [46, 47]. The convergence criterion was defined to 10^{-12} for continuity, velocity, and energy
 270 equations' residuals. Velocity-inlet and pressure-outlet boundary conditions were set at feed
 271 and permeate inlets and outlets, respectively. Wall and coupled boundary conditions were
 272 used at the upper and lower walls, and at the interface, respectively. The pressure inlet and
 273 outlet were also set at the air inlet and outlet, respectively [46, 47].



274

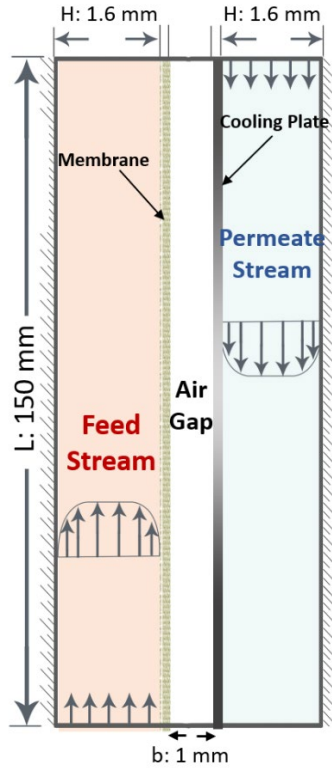
275 **Figure 3.** Flowchart illustrating the algorithm developed to include the effect of water vapour mass
 276 flux in the calculation of membrane temperature. n and k are the number of elements and iterations.
 277 Subscripts 'emp' and 'num' refer to empirical and numerical approaches [3].

278 A comprehensive parametric study of an AGMD system was undertaken. As presented in
 279 Table 1, the effect of inlet feed and permeate temperature, inlet velocity, feed concentration,
 280 and membrane characteristics for counter-current flow configuration with regards to water
 281 flux, CPC, TPC, and thermal efficiency of an AGMD system were explored. The baseline
 282 geometry to model an AGMD was sketched in Figure 4.

283 **Table 1.** Baseline and operating conditions for different parametric study of AGMD system

	Feed inlet temperature [°C]	Permeate inlet temperature [°C]	Inlet velocity [m/s]	Feed concentration [g/l]	Air gap thickness [mm]	Channel length [mm]
Baseline condition	60	25	0.05	10	1	150
Feed inlet temperature study	40-80	25	0.05	10	1	150
Inlet velocity study	60	25	0.005-0.2	10	1	150
Feed concentration study	60	25	0.05	0-250		150
Air-gap thickness study	60	25	0.05	10	0.2-5	150
Commercial Membranes	60	25	0.05	10	1	150

284



285

286 **Figure 4.** Schematic of flow configuration, counter-current operation, as a baseline for AGMD system
 287 (not to scale). *L*, length of the channels; *H*, width of the feed and permeate channel;
 288 *b*, air-gap channel thickness.

289 2.3. System Performance Metrics

290 2.3.1. Temperature Polarisation Coefficient

291 To assess the convective heat flux in the flow channels and the effect of temperature
 292 boundary layer and temperature polarisation, the TPC was calculated [48]. The TPC is defined
 293 as the ratio of the temperature difference between membrane feed side and condensate film
 294 side to the temperature difference between the bulk feed and the bulk permeate, as follows
 295 [48]:

$$TPC = \frac{T_{f,m} - T_{film}}{T_{f,b} - T_{p,b}} \quad (23)$$

296 where $T_{f,m}$ and T_{film} , represent the feed membrane temperature and film temperature, $T_{f,b}$
 297 and $T_{p,b}$ are the bulk feed and permeate temperature, respectively. TPC=1 indicates no
 298 temperature polarisation and high convective heat flux, and TPC=0 indicates high polarisation
 299 effect.

300 2.3.2. Concentration Polarisation Coefficient

301 To characterise concentration polarisation and measure the lateral mass concentration in
 302 the feed-side channel, CPC is calculated, as follows [48]:

$$CPC = \frac{C_{f,m}}{C_{f,b}} \quad (24)$$

$$C_{f,m} = C_{f,b} \exp\left(\frac{(J_w)_{m-ag}/\rho_f}{K_s}\right) \quad (25)$$

303 where $C_{f,m}$ and $C_{f,b}$ represents the concentration on the surface of the membrane feed-side
 304 and bulk feed fluid, respectively. ρ_f and K_s are the density and mass transfer coefficients of
 305 salt, respectively. $CPC=1$ indicates no concentration polarisation, and as CPC increases, the
 306 concentration polarisation effect increases.

307 2.3.3. Thermal Efficiency

308 Thermal efficiency defines the ratio of the latent heat of evaporation to the total heat
 309 transfer across the membrane and air-gap, as follows:

$$q''_{fg} = (J_w)_{m-ag} h_{fg} \quad (26)$$

$$q''_k = h_{am}(T_{f,m} - T_{film}) \quad (27)$$

$$\eta_t = \frac{q''_{fg}}{q''_{fg} + q''_k} \quad (28)$$

310 where q''_k , q''_{fg} , and η_t are the conduction heat transfer flux, phase change heat transfer
 311 flux, and thermal efficiency, respectively.

312 3. Results and Discussion

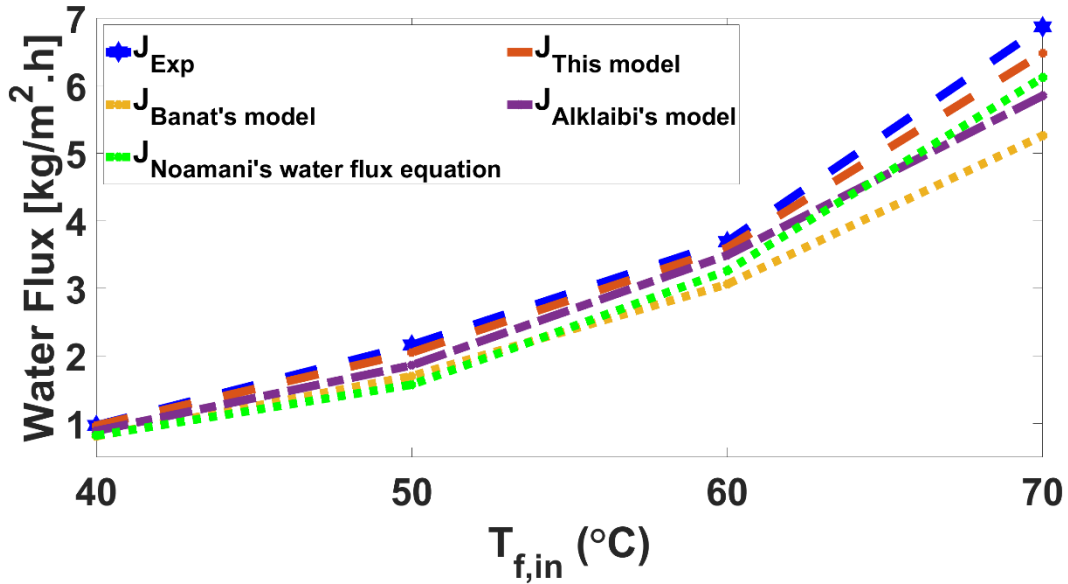
313 First, the developed model was validated against the experimental data [5, 14, 49]. Second,
 314 the influence of operating conditions including inlet temperature, velocity (Reynolds
 315 number), feed concentration, membrane properties including pore diameter, membrane
 316 thickness, porosity on the permeate flux, thermal efficiency, temperature, and concentration
 317 polarisation coefficients were investigated. Moreover, twenty-two commercially-available
 318 membranes, commonly used in the literature, were evaluated in terms of system
 319 performance metrics to assess the suitability of these membranes for AGMD application.
 320 Finally, AGMD was compared to DCMD under the same condition in terms of system
 321 performance metrics and downstream variation of permeate flux, in order to assess the
 322 downstream effect on the performance of MD systems.

323 3.1. Model Validation

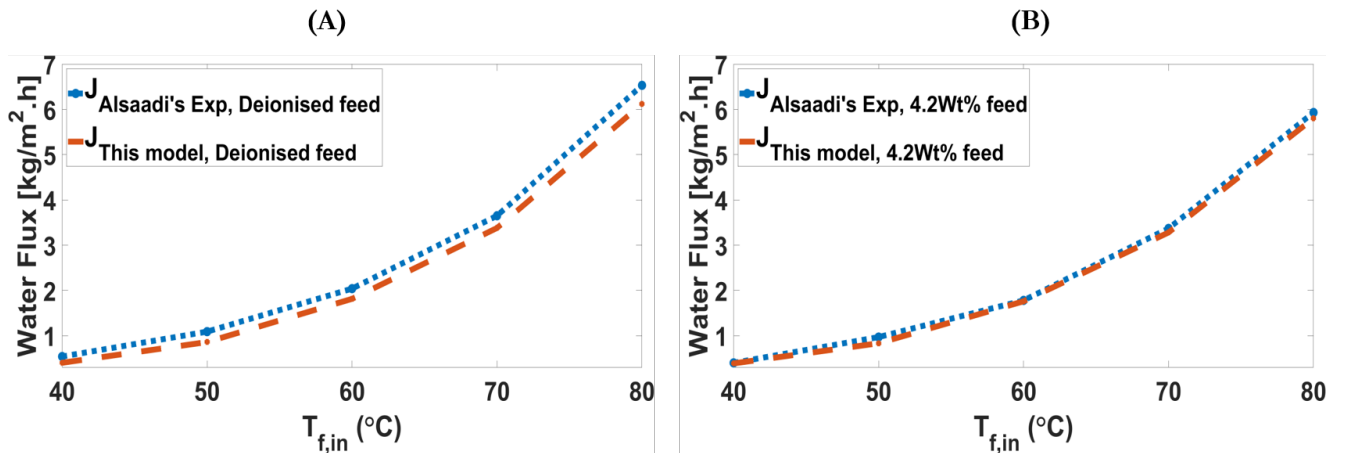
324 Four levels of structured quadrilateral mesh type were generated for the baseline condition
 325 and geometry to perform grid independence studies. The 220×150 mesh was chosen
 326 because the 250×150 mesh produced an insignificant (1%) error for the temperature and
 327 velocity values, as reported in the previous work [3].

328 The water flux results for different inlet feed temperatures were validated by comparison
 329 with Banat's experimental results [49]. As shown in Figure 5, they were in good agreement,
 330 within less than 4% deviation from the experimental results. It was shown that this model

331 improved the AGMD model compared to Banat's and Alklaibi's model [20], which are within
 332 approximately 20% and 10% deviation, respectively. This model was also compared with an
 333 alternate model using the water flux equation provided by Naomani et al. [12]. Our self-
 334 sustained water flux equation improved the water flux prediction from 15% to less than 4%
 335 deviation. As shown in Figure 6 and 7, this new model was also validated by comparison with
 336 Alsaadi's [14] and Xu's [5] experimental results, which were in good agreement. In the
 337 reported experiments, water permeate flux was recorded over 4 hours and measured with
 338 an uncertainty of ± 0.01 g. From consideration of effective membrane area, it was concluded
 339 that all models were beyond the uncertainty limits.

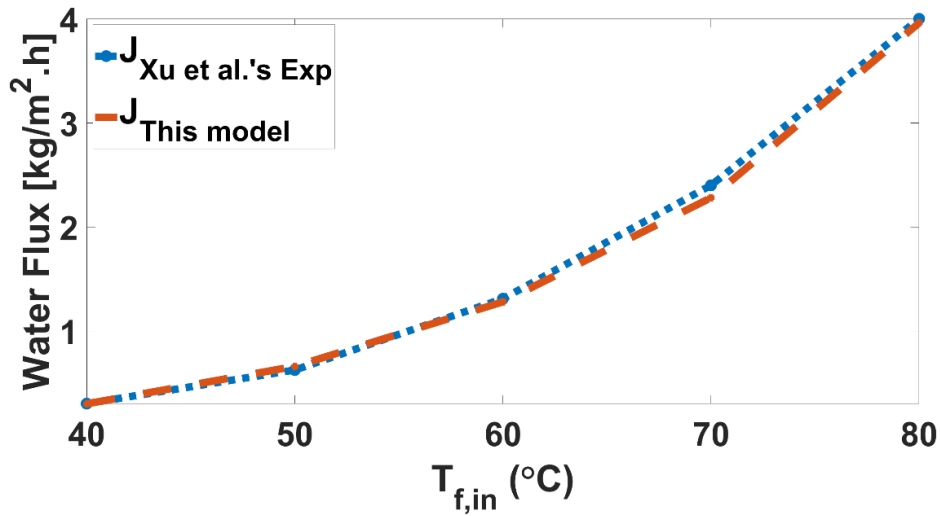


340
 341 **Figure 5.** The influence of feed temperature on the water permeate flux, showing the difference
 342 between Banat's experiments, this model ($D < 0.04$), Banat's model ($D < 0.2$), Alklaibi's model ($D < 0.1$),
 343 and alternate model when we used Noamani's water flux model ($D < 0.15$). The deviation from
 344 experimental results was calculated by $D = \frac{1}{n} \sum_i^n \frac{|J_{model_i} - J_{Exp_i}|}{J_{Exp_i}}$. The following condition were applied:
 345 Flow regime: Counter-current, $T_{p,in} = 20^\circ\text{C}$, $Q_{in} = 5.5$ L/min, $H = 2$ mm, $L = 130$ mm, $b = 3.5$ mm, $\delta =$
 346 0.11 mm, $\epsilon = 0.75$, $\delta_{cp} = 1.5$ mm, $d_p = 0.45$ μm , PVDF membrane Type, membrane area = 160 cm^2



347
 348 **Figure 6.** The influence of feed temperature on the water permeate flux, in comparison with Alsaadi's
 349 experiment [14]. (A). Deionised feed water ($D < 0.1$). (B) 4.2 Wt% feed water ($D < 0.05$). The following

350 condition were applied: Flow regime: Co-current, $T_{p,in} = 20^\circ\text{C}$, $Q_{in} = 1.5 \text{ L/min}$, $H=2 \text{ mm}$, $L=100$
 351 mm , $b=9 \text{ mm}$, $\delta = 100 \mu\text{m}$, $\epsilon = 0.8$, $\delta_{cp} = 0.25 \text{ mm}$, $d_p = 0.2 \mu\text{m}$, PTFE membrane Type, membrane
 352 area= 50 cm^2



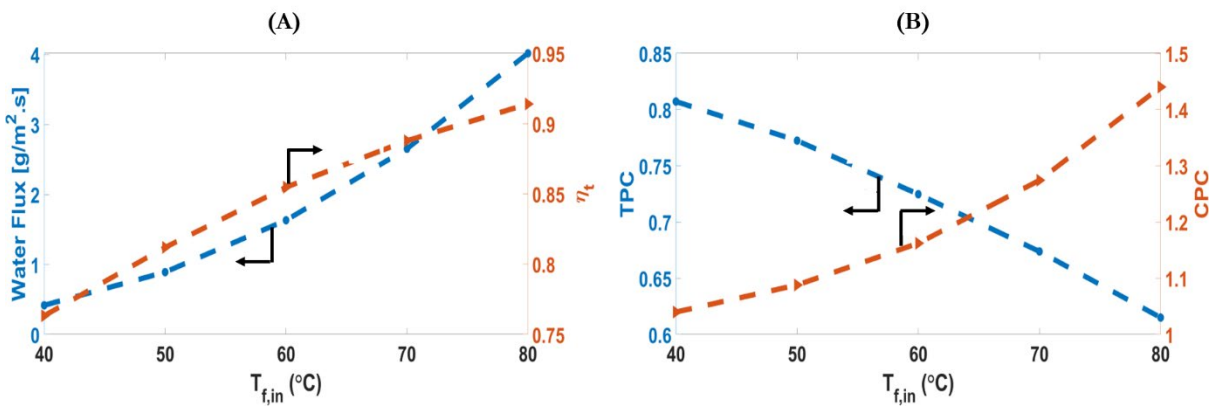
353

354 **Figure 7.** The influence of feed temperature on the water permeate flux, in comparison with Xu's
 355 experiment [5] ($D<0.03$). The following condition were applied: Flow regime: Counter-current, $C_{in} =$
 356 90 g/l , $T_{p,in} = 20^\circ\text{C}$, $U_{in,f} = 0.06 \text{ m/s}$, $U_{in,p} = 0.07 \text{ m/s}$ $H=2 \text{ mm}$, $L=100 \text{ mm}$, $b=10 \text{ mm}$, $\delta =$
 357 $166 \mu\text{m}$, $\epsilon = 0.687$, $\delta_{cp} = 0.25 \text{ mm}$, $d_p = 0.2 \mu\text{m}$, PTFE membrane Type, membrane area= 50 cm^2

358 3.2. Influence of Operating Conditions

359 3.2.1. Inlet Temperature

360 To study the influence of inlet temperature, a counter-current arrangement was modelled
 361 for the inlet temperatures $40 \leq T_f \leq 80^\circ\text{C}$. All other parameters were set as constant at the
 362 baseline condition (Table 1).



363

364 **Figure 8.** (A) Variation of mean water flux and thermal efficiency with varying inlet feed temperatures
 365 of a AGMD system. (B) Variation of TPC and maximum of CPC with varying inlet feed temperatures of
 366 a AGMD system.

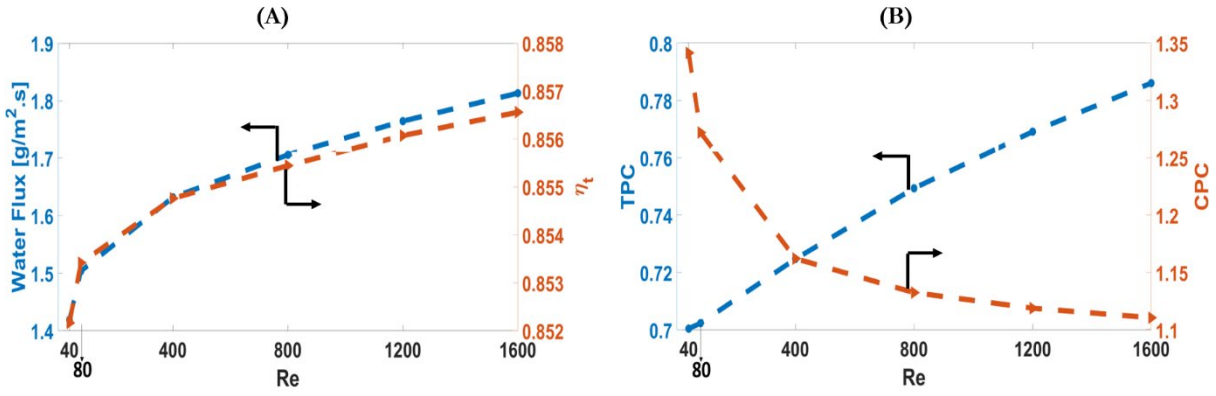
367 Figure 8 shows the effect of inlet feed temperature on the water permeate flux, thermal
 368 efficiency, TPC, and CPC. Equation (15) showed water flux (J_w) was a logarithmic function of
 369 vapour pressure on the feed membrane ($P_{v,fm}$) and film ($P_{v,film}$) sides; which both were an

370 exponential function of temperature (Equation [A19-A20]). Therefore, as the inlet feed
371 temperature increased, (J_w) increased exponentially. A two-fold increase of inlet feed
372 temperature from 40°C to 80°C, was found to increase J_w by a factor of 9.5, from 0.42 to 4.01
373 ($\text{g}/\text{m}^2\text{s}$); and the thermal efficiency was increased from 76% to 91%. The increase in thermal
374 efficiency occurred due to the increase of the phase change heat transfer flux rate (dependent
375 on J_w) compared to the conduction heat transfer flux rate [dependent on $(T_{f,m} - T_{film})$].
376 Figure 8 (B) shows temperature and concentration polarisation effects increased as the inlet
377 feed temperature increased: TPC decreased from 0.81 to 0.61 and CPC increased from 1.04
378 to 1.44, respectively. With increasing inlet feed temperature from 40°C to 80°C, the bulk
379 temperature ($T_{f,b} - T_{p,b}$) and J_w increased 3.6-fold and 9.5-fold, respectively. Therefore, the
380 ratio of thermal resistance of membrane and air gap channel to the overall thermal resistance
381 of the AGMD system decreased, and consequently TPC decreased. CPC is an exponential
382 function of J_w and K_s^{-1} . K_s , mass transfer of salt in water, increased with increasing of
383 temperature because the density and dynamic viscosity decreased, resulting in a higher
384 Sherwood number and a lower Schmidt number. Therefore, although J_w increased 9.5-fold,
385 CPC increased only by 38%.

386 3.2.2. Reynolds Number

387 To examine the effects of the inlet velocity, a counter-current arrangement of an AGMD
388 system was modelled for $0.005 \leq V_{in} \leq 0.2$ m/s, corresponding to the laminar Reynolds
389 numbers of $40 \leq Re \leq 1600$. All other parameters were maintained at the baseline
390 condition.

391 Figure 9 shows the effect of laminar Reynolds number on the water permeate flux, thermal
392 efficiency, TPC, and CPC. An increased Reynolds number decreased the thermal boundary
393 layer, which reduced the temperature and concentration polarisation effects [Figure 9(B)]. As
394 a result a higher water flux through the system was observed [Figure 9(A)]. By increasing the
395 Reynolds number from 40 to 1600, the water permeate flux increased 28%, from 1.419 to
396 1.813 ($\text{g}/\text{m}^2\text{s}$), and the thermal efficiency increased only slightly. As described above, with
397 an increase of Reynolds number from 40 to 1600, the temperature polarisation effect
398 decreased due to an increase in turbulence. Therefore TPC increased from 0.7 to 0.79. It was
399 shown that although water permeate flux increased, the CPC decreased to some extent from
400 1.31 to 1.11. As explained above, two opposing factors, water flux and the solute convection
401 mass transfer coefficient, affected the CPC. With an increase of Reynolds number, the
402 dominant effect of the solute mass transfer increase over water flux increase on the CPC
403 resulted in a decrease in CPC.

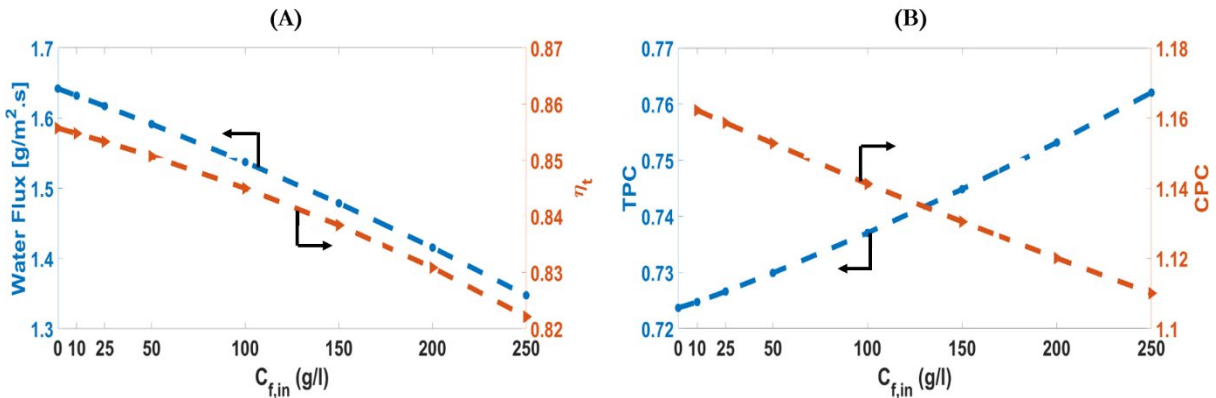


404

405 **Figure 9.** (A) The effect of the varying laminar Reynolds number of an AGMD system on the mean water
 406 flux and thermal efficiency. (B) Variation of TPC and maximum CPC with varying laminar Reynolds
 407 number in an AGMD system.

408 3.2.3. Inlet Concentration

409 To investigate the influence of inlet feed concentration, a counter-current arrangement of a
 410 AGMD system was modelled for the inlet feed concentration $0 \leq C_f \leq 250$ g/l with all other
 411 parameters maintained at the baseline condition.



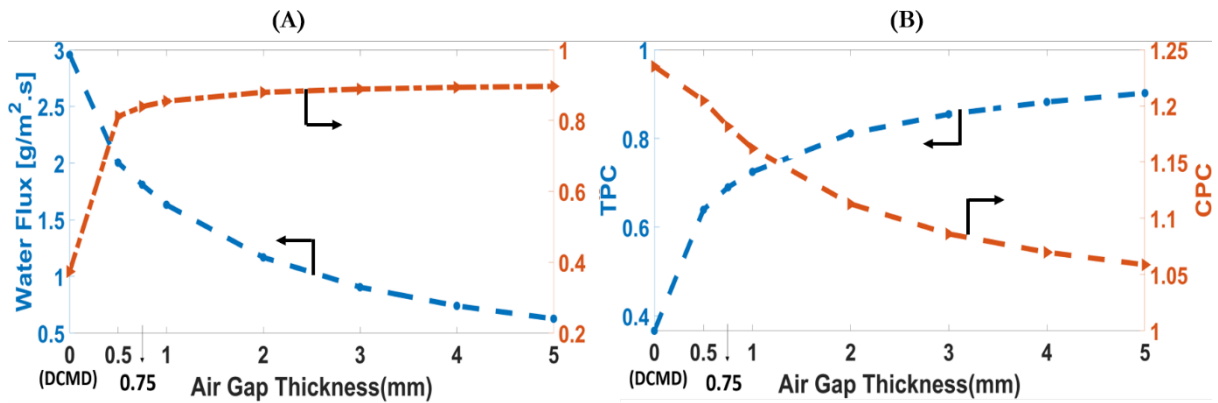
412

413 **Figure 10.** (A) Variation of mean water flux and thermal efficiency with varying inlet feed
 414 concentrations of an AGMD system. (B) Variation of TPC and maximum of CPC with varying inlet feed
 415 concentrations of an AGMD system.

416 Figure 10 (A) shows the decrease in water flux from 1.642 (g/m²s) for $C_f = 0$ g/l to 1.35
 417 (g/m²s) for $C_f = 250$ g/l. This behaviour occurred due to a decrease in vapour pressure
 418 difference, which was the minus quadratic function of molality [Equation (A21)]. The
 419 decreased water flux resulted in a decrease in CPC from 1.16 to 1.11, as seen in Figure 10 (B).
 420 Decreasing the water flux resulted in a decrease of q''_{fg} ; therefore, η_t decreased from 0.856
 421 to 0.822. By increasing C_f from 0 g/l to 250 g/l, the TPC increased from 0.724 to 0.762. This
 422 was because when Equation (2) was divided by $T_{f,b} - T_{p,b}$, at the fixed bulk temperature, the
 423 decreased water flux resulted in higher thermal resistance for the phase change heat transfer,
 424 and consequently, the TPC increased.

425 3.2.4. Air Gap Thickness

426 To examine the effect of air gap thickness, a counter-current arrangement of an AGMD
 427 system was modelled ranging from $0.5 \leq b \leq 5$ mm with all other parameters maintained at
 428 the baseline condition. To compare AGMD and DCMD processes, we have included the case
 429 of $b = 0$ (DCMD process, which is explained in Section 3.4).



430
 431 **Figure 11.** (A) Variation of mean water flux and thermal efficiency with varying air gap thickness of a
 432 AGMD system. (B) Variation of TPC and maximum of CPC with varying air gap thickness of a AGMD
 433 system.

434 Figure 11 (A) illustrated that the water flux decreased from 2 (g/m²s) for $b = 0.5$ mm to 0.6
 435 (g/m²s) for $b = 5$ mm. This was because increasing air gap thickness created further mass
 436 transfer resistance, thus reducing the water permeate flux. However, situation also led to a
 437 6% increase in thermal efficiency from 0.81 to 0.87 due to the decrease in heat loss along the
 438 module. This was because the decreased rate of conduction heat transfer q''_k was more than
 439 a phase change heat transfer q''_{fg} since the air heat transfer coefficient (h_a) significantly
 440 decreased. Figure 11 (B) illustrates that both temperature and concentration polarisation
 441 effects significantly reduce with an increasing air gap thickness. When b increased from 0.5
 442 mm to 5 mm, TPC increased from 0.64 to 0.9 and CPC decreased from 1.2 to 1.05.

443 3.3. Influence of Membrane Properties and Commercial Membranes

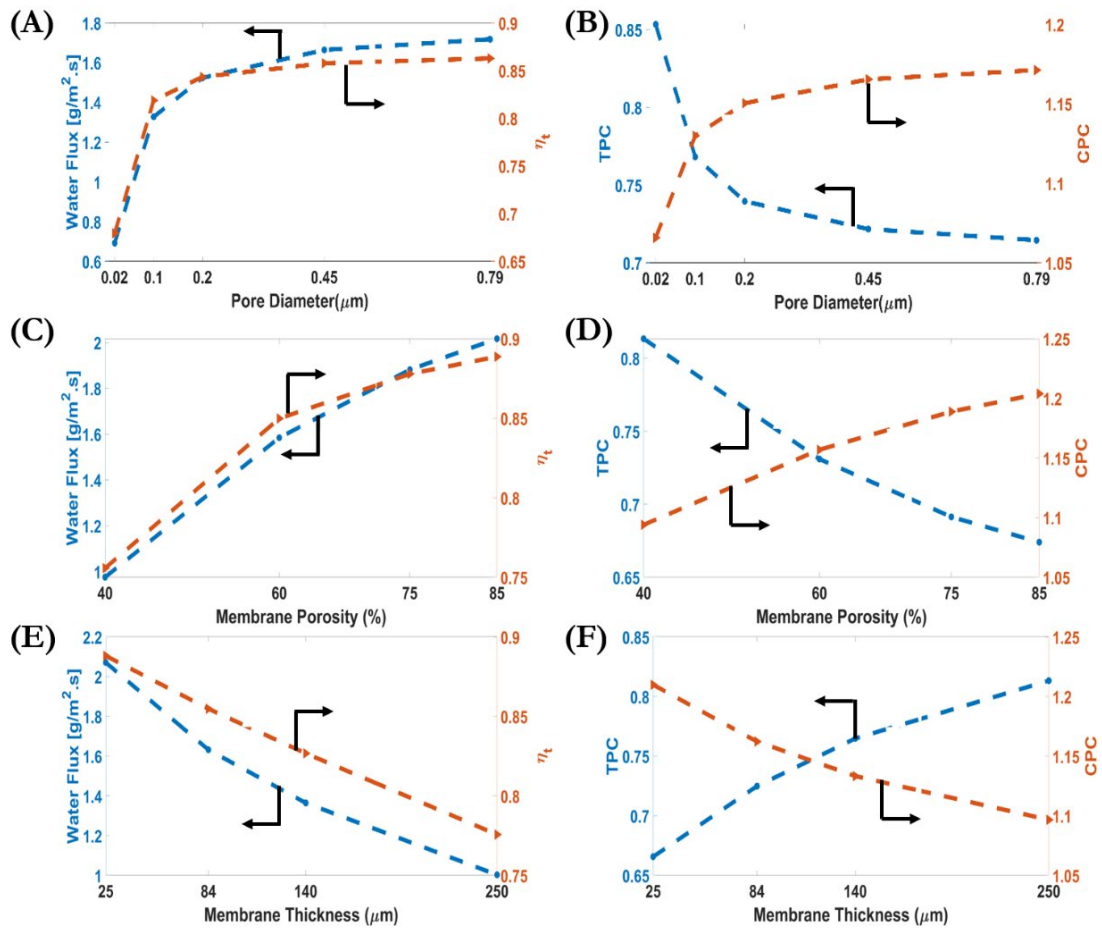
444 3.3.1. Membrane Properties

445 To examine the effect of membrane properties, a counter-current arrangement of an AGMD
 446 system was modelled with different membrane pore diameter, porosity, and membrane
 447 thickness, ranging from $0.02 \leq d_p \leq 0.79$ μm , $40\% \leq \epsilon \leq 85\%$, and $25 \leq d_p \leq 250$ μm ,
 448 respectively while all other parameters were maintained at the baseline condition.

449 Figure 12 shows the variation of water permeate flux, thermal efficiency, TPC, and CPC with
 450 varying membrane properties, including pore diameter, porosity, and thickness. When the
 451 pore diameter was increased from 0.02 to 0.79 μm , the water flux and the thermal efficiency,
 452 increased from 0.69 to 1.72 (g/m²s) and 0.68 to 0.86, respectively. Both temperature and
 453 concentration polarisation effects intensified with increasing membrane pore diameter. More
 454 specifically, TPC decreased 17% from 0.85 for 0.02 μm to 0.71 for 0.79 μm and CPC increased
 455 9% from 1.07 for 0.02 μm to 1.17 for 0.79 μm . Figure 12 (A,B) showed that the rate of increase
 456 in water flux, thermal efficiency, temperature, and concentration polarisation effects from

457 0.02 to 0.1 μm was higher than the range 0.1 to 0.79 μm . This was because the membrane
 458 pore diameter was less than the mean free path length. Consequently, the mass transfer
 459 mechanism was predominantly Knudsen diffusion. Figures 12 (C, D) show that with increasing
 460 membrane porosity from 40% to 85%, the water flux and the thermal efficiency increased
 461 from 0.97 to 2.01 $\text{g}/\text{m}^2\text{s}$ and 0.76 to 0.89, respectively. However, both the temperature and
 462 concentration polarisation also increased. TPC decreased from 0.81 to 0.67 and CPC increased
 463 from 1.09 to 1.2. Figures 12 (E, F) showed that with increasing membrane thickness δ , the
 464 membrane mass transfer resistance increased, leading to less water flux and, consequently,
 465 less temperature and concentration polarisation effects. As shown, increasing membrane
 466 thickness from 25 to 250 μm reduced the water flux and the thermal efficiency from 2.07 to
 467 1 $\text{g}/\text{m}^2\text{s}$ and 0.89 to 0.78, respectively. Moreover, TPC increased from 0.67 to 0.81 and the
 468 CPC decreased from 1.21 to 1.1.

469



470

471 **Figure 12.** (A) Variation of mean water flux and thermal efficiency with varying membrane pore
 472 diameter of an AGMD system. (B) Variation of TPC and maximum of CPC with varying membrane pore
 473 diameter of an AGMD system. (C) Variation of mean water flux and thermal efficiency with varying
 474 membrane porosity of an AGMD system. (D) Variation of TPC and maximum of CPC with varying
 475 membrane porosity of an AGMD system. (E) Variation of mean water flux and thermal efficiency with
 476 varying membrane thickness of an AGMD system. (F) Variation of TPC and maximum of CPC with
 477 varying membrane thickness of an AGMD system.

478 3.3.2. Commercial Membranes

479 To compare the effect of the membrane parameters on the AGMD performance, a counter-
 480 current arrangement of an AGMD system was modelled for 22 commercially available
 481 membranes [Table 2], while all other parameters were maintained at the baseline condition.

482 **Table 2.** Membranes selected for this study, and characteristics provided by their manufacturers-50/
 483 [52].

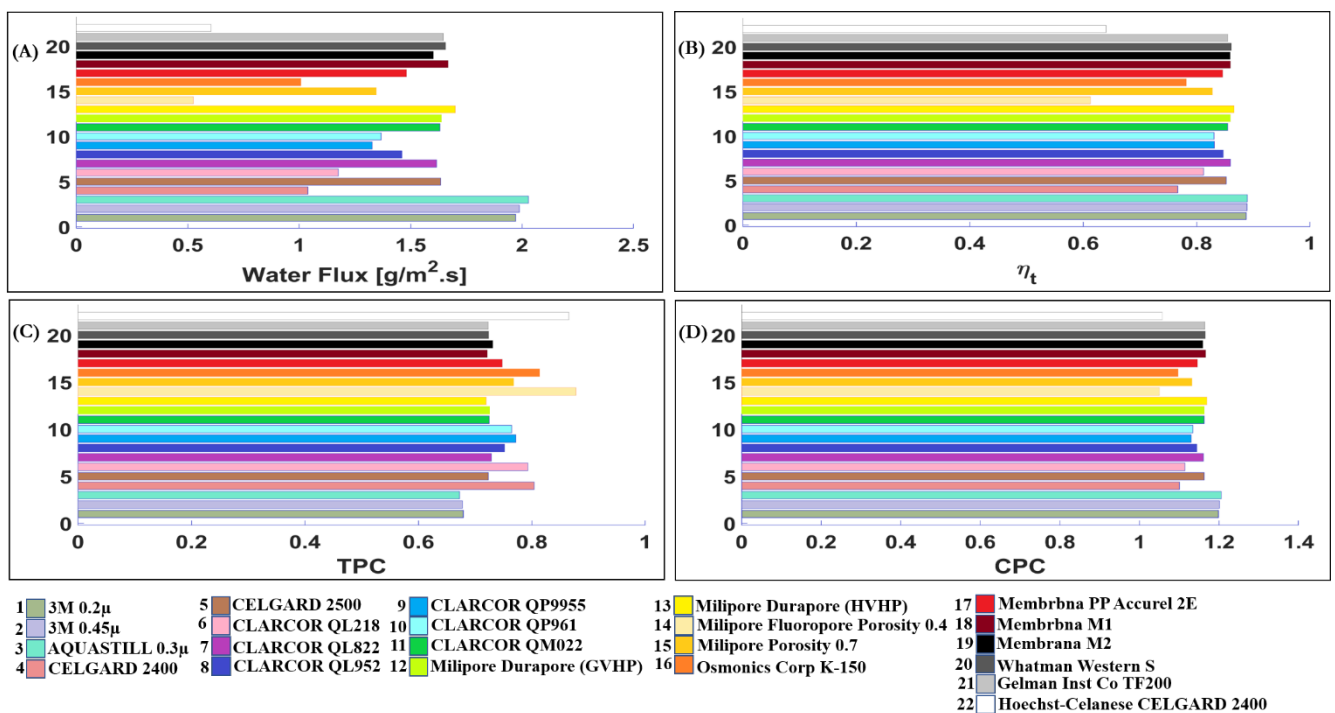
Manufacturer	Model Number	Membrane Type	Nominal Pore Size (µm)	Thickness (µm)	Porosity (%)
3M	0.2 µm	PP	0.59	110	85
3M	0.45 µm	PP	0.79	110	85
AQUASTILL	0.3 µm	PE	0.3	76	85
CELGARD	2400	PP	0.043	25	41
CELGARD	2500	PP	0.064	25	55
CLARCOR	QL218	PTFE	0.2	280	75
CLARCOR	QL822	PTFE	0.45	165	75
CLARCOR	QP952	PTFE	0.45	223	75
CLARCOR	QP9955	PES	0.2	216	75
CLARCOR	QP961	PES	0.1	140	75
CLARCOR	QM022	PTFE	0.36	84	62
Millipore	Durapore (GVHP)	PVDF	0.22	125	75
Millipore	Durapore (HVHP)	PVDF	0.45	140	75
Millipore	Fluoropore	PTFE	0.22	175	40
Millipore	Fluoropore	PTFE	0.22	175	70
Osmonics Corp	k-150	PTFE	0.1	260	75
Membrana, Germany	PP Accurel 2E	PP	0.2	163	75
Membrana, Germany	M1	PP	0.2	91	70
Membrana, Germany	M2	PP	0.45	170	75
Whatman, Germany	Westran S	PVDF	0.2	121	76
Gelman Inst Co	TF200	PTFE	0.2	60	60
Hoechst-Celanese	CELGARD 2400	PP	0.02	25	38

484

485 Figure 13 showed the water flux, thermal efficiency, TPC, and CPC for each of the 22 different
 486 membranes. It was shown that different membrane properties can significantly affect AGMD
 487 performance. The AQUASTILL membrane showed the most effective performance compared
 488 to the other 22 membranes because of the high porosity, 85%, and suitable thickness, 76 µm.
 489 The water flux, thermal efficiency, TPC, and CPC of the AGMD system with the AQUASTILL
 490 membrane were 2.03 g/m²s, 0.89, 0.67, and 1.2, respectively. Although AQUASTILL had
 491 lower pore diameter compared to both 3M 0.45 µm and 0.2 µm membranes, it benefited
 492 from smaller membrane thickness. A comparison of Membrana M2 with Membrana M1
 493 showed that although Membrana M2 had greater pore diameter because of the increased
 494 thickness, both membranes exhibited equal performance. A comparison between CLARCOR
 495 QM022 and Millipore Durapore (GVHP) showed a significant effect of porosity on the AGMD
 496 performance. Although CLARCOR QM022 benefited from 40% higher pore diameter and 50%
 497 lower thickness, it had 21% lower porosity, it performed similarly to Millipore Durapore
 498 (GVHP). For CLARCOR QM022 and Millipore Durapore (GVHP), water flux, thermal efficiency,
 499 TPC, and CPC of AGMD system were 1.63 g/m²s, 0.85, 0.72, and 1.16, respectively. The
 500 performance of AGMD with the Hoechst-Celanese membrane revealed that although the
 501 system benefited from the low temperature and concentration polarisation effects with TPC
 502 and CPC of 0.86 and 1.05, respectively; it had a lower water flux, 0.6 g/m²s. This situation
 503 occurred due to the small pore diameter as well as porosity (0.02 µm and 38%, respectively).

504 Analysing all 22 membranes showed that Millipore Fluoropore Porosity 0.4 benefited from
 505 the lowest temperature and concentration polarisation effects, with TPC and CPC of 0.88 and
 506 1.05, respectively. However, it suffered from the lowest water flux and the lowest thermal
 507 efficiency, 0.52 g/m²s and 0.61, respectively. These results revealed that the 3M 0.45 μm
 508 membrane with 34% higher pore diameter compared to 3M 0.2 μm membrane shows slight
 509 improvement in an AGMD system. Comparison between two membranes from the
 510 manufacturer CELGARD showed that increasing pore diameter by 49% from 0.043 to 0.064
 511 μm, and 14% porosity from 41% to 55%, improved the performance of an AGMD system in
 512 terms of water flux and thermal efficiency from 1.039 to 1.635 g/m²s and 0.77 to 0.85,
 513 respectively. Analysing the membranes manufactured by CLARCOR illustrated that the
 514 QM022 model number with 0.36 μm pore diameter, 84 μm thickness and 62% porosity
 515 performed most efficiently in an AGMD system in terms of water flux and thermal efficiency;
 516 which are 1.632 g/m²s and 0.85, respectively. A comparison between two membranes from
 517 Millipore revealed that Durapore (HVHP) (0.45 μm pore diameter, 140 μm thickness and 75%
 518 porosity) provided an increased water flux and thermal efficiency, which were 1.7 g/m²s and
 519 0.87, respectively. This occurred due to the higher porosity compared to the Fluoropore
 520 models and higher pore diameter than Durapore (GVHP).

521



522

523 **Figure 13.** A comparison of the performance of 22 commercially available membranes listed
 524 in Table 2: (A) Water flux, (B) Thermal efficiency η_t , (C) TPC, and (D) CPC.

525

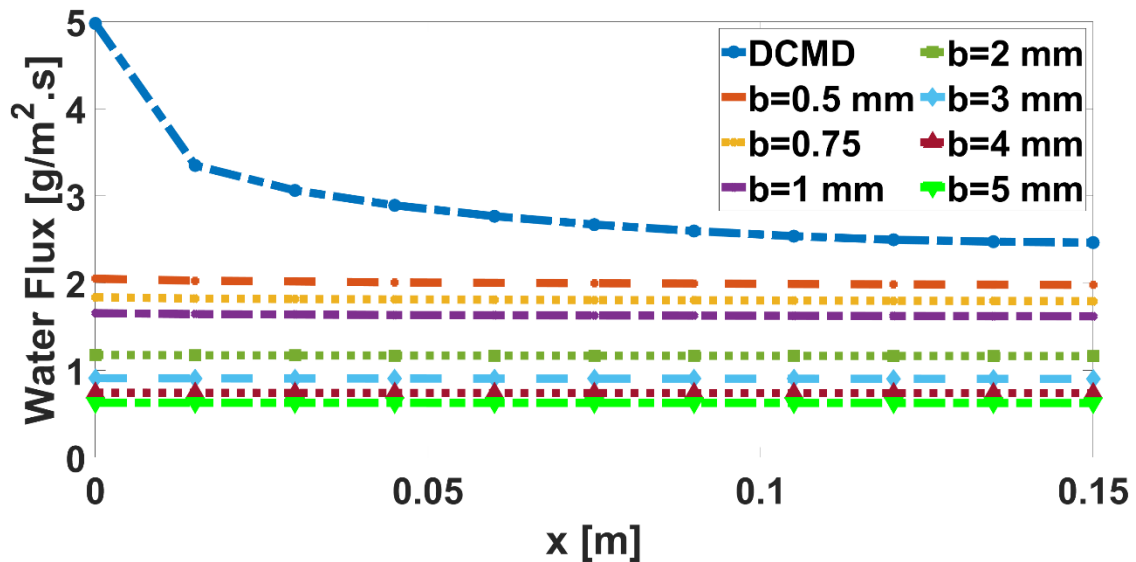
526 3.4. Comparative Study of AGMD and DCMD

527 In this section, in continuation of a previous study [3], DCMD and AGMD performance results
 528 were compared in terms of downstream water-flux variations and system performance

529 metrics including water flux, thermal efficiency, TPC, and CPC. A counter-current arrangement
530 of DCMD and AGMD was modelled for different Reynolds number in the range $40 \leq Re \leq$
531 1600 , and different air gap thickness as described in the Section 4.2.4. Results from a previous
532 study [3] revealed that the downstream variation of water flux significantly changed along the
533 module, thus reducing the DCMD system performance. This section focused on downstream
534 variations of water flux along the module to compare the DCMD and AGMD systems.

535 Figure 11 showed that the DCMD process provided significantly higher water flux compared
536 to the AGMD process. This was because the air gap channel's mass and heat transfer
537 resistances led to a decrease in driving force in an AGMD system. Figure 11 showed that the
538 water flux for DCMD was $2.95 \text{ g/m}^2\text{s}$, while for AGMD with 0.5 mm air-gap thickness it was 2
539 $\text{g/m}^2\text{s}$ and with 5 mm air-gap thickness decreased to $0.63 \text{ g/m}^2\text{s}$. On the other hand, the
540 thermal efficiency of AGMD was higher than DCMD because the air gap channel caused a
541 lower heat loss. Figure 11 showed that η_t was 0.37 for the DCMD system, while it was 0.81
542 for AGMD with 0.5 mm air gap thickness and increases to 0.89 for AGMD with 5 mm air gap
543 thickness. It was also shown that AGMD systems benefit from lower temperature and
544 concentration polarisation effects. Figure 11 illustrated that TPC for DCMD is 0.37 , while it
545 was 0.64 and 0.9 for AGMD with b of 0.5 and 5 mm , respectively. CPC of 1.24 for DCMD was
546 larger than AGMD, which was 1.05 for b of 5 mm .

547 Figure 14 illustrated that contrary to AGMD, DCMD suffered from a considerable reduction of
548 the water flux along the module. The water flux for DCMD decreased 50% from $4.98 \text{ g/m}^2\text{s}$
549 at the inlet to $2.465 \text{ g/m}^2\text{s}$ at the exit, while for AGMD with 1mm air gap thickness it
550 decreased 2% from $1.655 \text{ g/m}^2\text{s}$ to $1.62 \text{ g/m}^2\text{s}$. Figure 15 showed that with a reduced
551 Reynolds number, the downstream variation of DCMD significantly increased, from a 30%
552 reduction (from 5.943 to $4.15 \text{ g/m}^2\text{s}$, for $Re=1600$) to 77% reduction (from 2.966 to 0.683
553 $\text{g/m}^2\text{s}$, for $Re=40$). As described above, although the water flux of DCMD was higher than
554 AGMD, as shown in Figure 15, the reduction of water flux along the system for DCMD reached
555 a point lower than for AGMD. Therefore, the insignificant variation of water flux along the
556 AGMD was a considerable advantage of AGMD over DCMD. In conclusion, although AGMD
557 provides lower water flux compared to DCMD, it outperformed in terms of thermal efficiency,
558 TPC, CPC, and fewer downstream variations. Figure 16 shows with an increase of module
559 length, the water flux decreased. In the case that Re and the air-gap thickness were 40 and
560 0.5 mm , respectively; the water flux for AGMD with module length of 100 mm decreased 86%
561 from $1.84 \text{ g/m}^2\text{s}$ at the inlet to $1.585 \text{ g/m}^2\text{s}$ at the exit. While for AGMD with module length
562 of 500 mm it decreased 56% from $1.335 \text{ g/m}^2\text{s}$ to $0.754 \text{ g/m}^2\text{s}$. In conclusion, Re number
563 which was relative to the inlet velocity and channel height, air-gap thickness and module
564 length determined the value of downstream variation of water flux in AGMD.

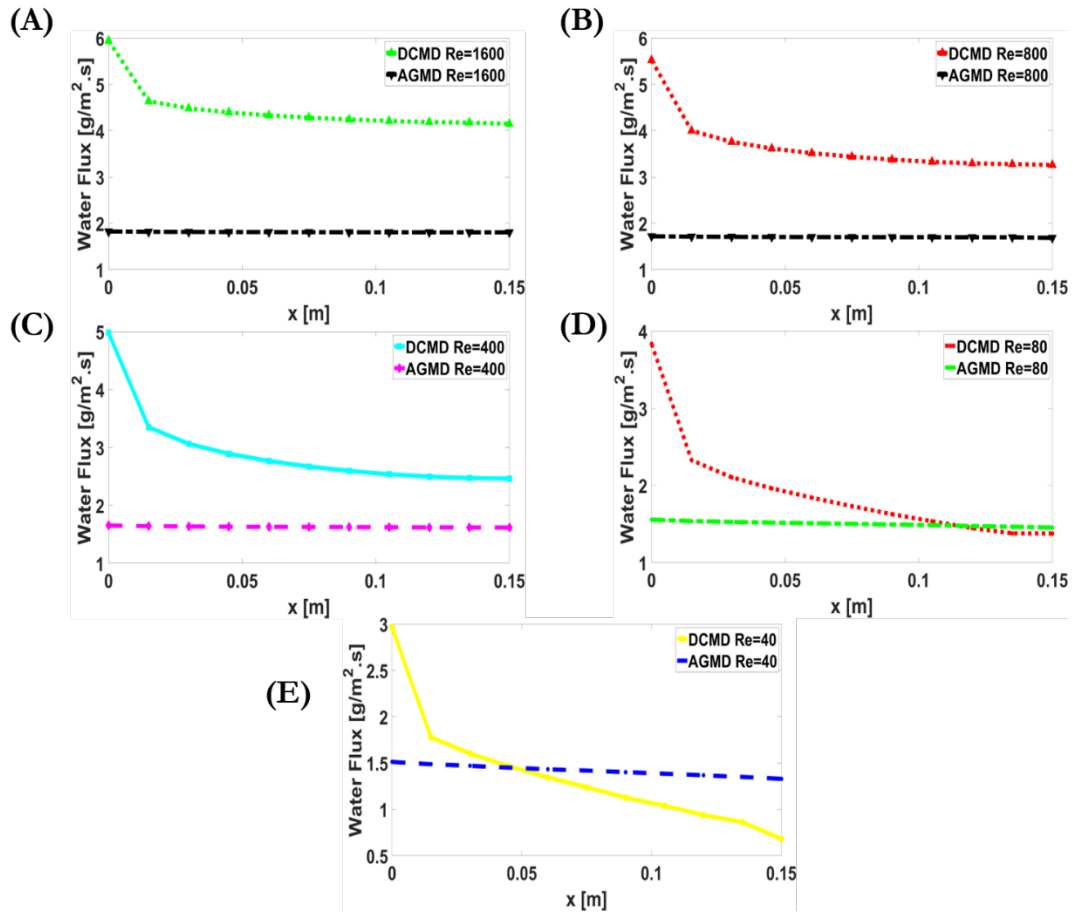


565

566 **Figure 14.** Downstream variations of water flux for DCMD and AGMD systems with different air gap
 567 thickness for the baseline condition. ($L=150$ mm, $H=1.6$ mm, CLARCOR, QM0200 membrane type,
 568 $Re=400$ ($U_{in} = 0.05$ m/s), $C_{f,in}=10$ g/l, $T_{f,in}=60$ °C $T_{p,in}=25$ °C)

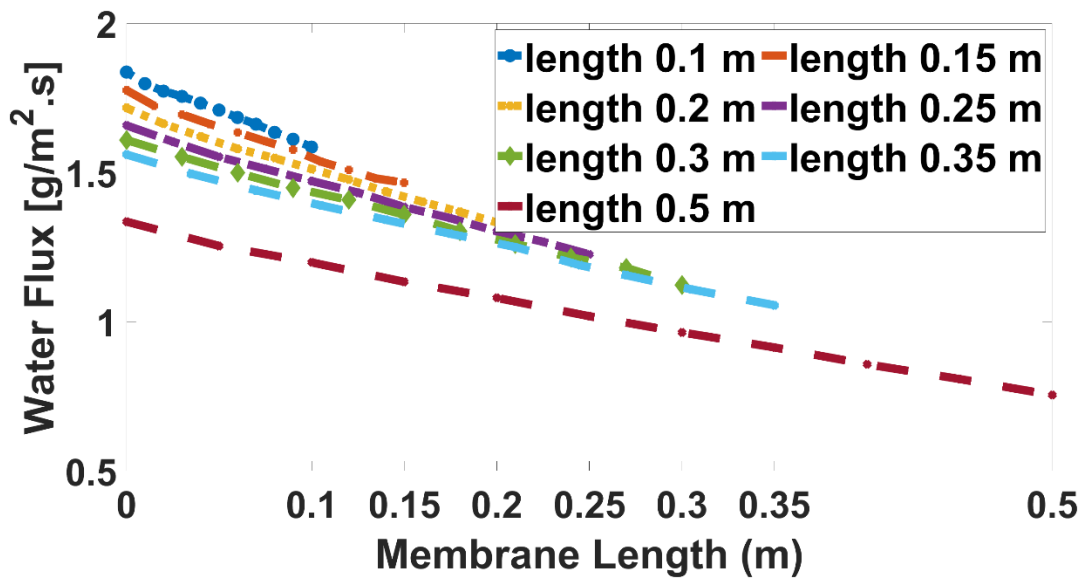
569 Table 3 showed that increasing inlet temperature had the most significant positive effect on
 570 water flux and thermal efficiency; however, it negatively affected temperature and
 571 concentration polarisation. Among the operating conditions, increasing the Reynolds number
 572 presented a positive effect on all the system performance, including higher water flux and
 573 lower temperature and concentration polarisation effects. Table 3 also revealed that
 574 increasing the inlet concentration and the increased air gap thickness yielded lower both
 575 temperature and concentration polarisation. The increased porosity and pore diameter
 576 significantly affected AGMD performance by increasing water flux and increasing both
 577 temperature and concentration polarisation effects.

578 Table 3 also showed that increased inlet temperature led to more significant changes in
 579 thermal efficiency and both temperature and concentration polarisation for DCMD compared
 580 to AGMD. A two-fold increase of inlet temperature from 40 °C to 80 °C increased the thermal
 581 efficiency and CPC, 20% and 76%, respectively and it decreased 46% TPC for a DCMD system;
 582 it increased thermal efficiency and CPC, 15.1% and 38%, respectively, and decreased TPC 26%
 583 for an AGMD system. The effect of Reynolds number on DCMD was higher than for the AGMD
 584 system. In detail, increasing Reynolds number from 40 to 1600 resulted in a 320% increase of
 585 water flux for DCMD, while it was 28% for AGMD. This increased Reynolds number yielded a
 586 200% increase of TPC, while for AGMD it was 12.3%. In general, the sensitivity of DCMD on
 587 changing operating conditions, among which the Reynolds number was the highest is more
 588 considerable than AGMD.



589

590 **Figure 15.** Comparison of variations in the downstream water flux (A DCMD and AGMD systems for
 591 $Re=1600$. (B) DCMD and AGMD systems for $Re=800$. (C) DCMD and AGMD systems for $Re=400$. (D)
 592 DCMD and AGMD systems for $Re=80$. (E) DCMD and AGMD systems for $Re=40$. ($L=150$ mm, $H=1.6$ mm,
 593 CLARCOR-QM0200 membrane type, $C_{f,in}=10$ g/l, $T_{f,in}=60$ °C $T_{p,in}=25$ °C, and $b=1$ mm for AGMD
 594 systems)



595

596 **Figure 16.** Downstream variations of water flux for AGMD systems with different length modules.
 597 the baseline condition. ($H=1.6$ mm, $b=0.5$ mm CLARCOR, QM0200 membrane type, $Re=40$ ($U_{in} =$
 598 0.005 m/s), $C_{f,in}=10$ g/l, $T_{f,in}=60$ °C $T_{p,in}=25$ °C)

599 **Table 3.** Parametric study of AGMD and DCMD systems. Operating conditions for AGMD provided in
600 Table 1 and for DCMD provided in Reference [3]. The plus and minus signs mean the increase and
601 reduction in the intended system performance metrics for each variation range, respectively.

Parameter Study		System Performance Metrics								
		Variation Range	Water Flux (J) [g/m ² s]		CPC		TPC		Thermal Efficiency (η_t)	
			AGMD	DCMD	AGMD	DCMD	AGMD	DCMD	AGMD	DCMD
Operating Conditions	Inlet Feed Temperature [°C]	40 → 80	+9.5-fold 0.42 → 4.02	10-fold 0.76 → 7.66	+38% 1.04 → 1.44	+76% 1.04 → 1.84	-26% 0.81 → 0.62	-46% 0.60 → 0.14	+15.1% 76.3 → 91.4	+20% 27 → 47
	Inlet Velocity [m/s] / Reynolds Number	0.005 → 0.2 / 40 → 1600	+28% 1.42 → 1.81	3.2-fold 1.4 → 4.46	-17% 1.34 → 1.12	-16% 1.36 → 1.17	+12.3% 0.7 → 0.79	2-fold 0.23 → 0.46	+0.4% 85.2 → 85.6	+1% 36.9 → 37.9
	Inlet Concentration [g/l]	0 → 250 / 10 → 250 (for CPC)	-18% 1.64 → 1.35	-17% 2.99 → 2.5	-4% 1.16 → 1.11	-7.3% 1.23 → 1.14	+5% 0.72 → 0.76	+41% 0.36 → 0.51	-3.4% 85.6 → 82.2	-7% 37 → 30
	Air Gap Thickness [mm]	0.5 → 5	AGMD -68% 2 → 0.63		AGMD -15% 1.235 → 1.05		AGMD +40% 0.64 → 0.9		AGMD +8% 81 → 89	
Membrane Properties	Membrane Thickness [μm]	25 → 250	-51.6% 2.07 → 1		-9.4% 1.21 → 1.097		+22% 0.67 → 0.81		-11.24% 88.8 → 77.56	
	Pore Diameter [μm]	0.02 → 0.79	+ 2.6-fold 0.66 → 1.72		+9% 1.07 → 1.17		-16% 0.85 → 0.71		+18% 68 → 86	
	Porosity [%]	40 → 85	+ 2.06-fold 0.98 → 2.02		+10% 1.09 → 1.2		-17% 0.81 → 0.67		+13% 76 → 89	

602

603 5. Conclusion

604 By improving a water permeate flux model and the inclusion of downstream variations of
605 AGMD and DCMD, this study reported a comprehensive analysis of AGMD and a comparative
606 study of AGMD and DCMD, in terms of water permeate flux, thermal efficiency, temperature,
607 and concentration polarisation effects. The results showed that the improved model was in
608 good agreement with the experimental results and an enhanced the prediction from 15% to
609 less than 4% deviation.

610 The results revealed that the performance of AGMD system is susceptible to the inlet feed
611 temperature, the Reynolds number, and the air gap thickness. When the inlet feed
612 temperature was doubled, the water flux, thermal efficiency, and CPC increased by 9.5-fold,
613 15.1%, and 38%, respectively, and TPC decreased by 26%. According to the results, water flux
614 and both temperature and concentration polarisation effects were treated similarly by
615 changing the operating conditions, excluding the Reynolds number. Although an air gap
616 thickness increase from 0.5 to 5 mm, caused a 68% reduction in the water flux, it decreased
617 both polarisation effects: A 15% reduction in CPC and a 40% increase in TPC. On the other
618 hand, by increasing Reynolds number from 40 to 1600, the water flux and thermal efficiency
619 increased by 28% and 1%, respectively. The adverse effects of both polarisations decreased
620 by a 17% reduction in CPC and 12.3% increase in TPC. Results also revealed that the
621 membrane properties can considerably affect the AGMD performance. It was shown that by
622 increasing porosity from 40 to 85%, water flux, thermal efficiency, was enhanced by 2.06-fold
623 and 13%, and undesirably both polarisations increased by a 10% increase in CPC and 17%
624 reduction in TPC. Analysing 22 different commercially available membranes revealed that
625 AQUASTILL membrane with 85% porosity and 76 μm thickness, showed the most effective
626 MD performance compared to the other commercially available membranes.

627 DCMD performance was shown to be more sensitive to the operating conditions compared
628 to AGMD performance. By increasing the Reynolds number from 40 to 1600, the water flux
629 and TPC changed 28% and 12.3%, respectively, for AGMD, while they changed 3.2-fold and 2-
630 fold, respectively, for DCMD. In addition, results showed that the DCMD system runs a
631 significantly higher water flux than AGMD; however, AGMD provides higher thermal
632 efficiency, and lower concentration and temperature polarisation effects in the same
633 condition. The water flux of DCMD was 80% more than AGMD with air gap thickness of 1mm;
634 however, the thermal efficiency and TPC of DCMD were 51% and 49% lower than the value
635 of AGMD with air gap thickness of 1mm. The results also showed that, unlike the AGMD,
636 DCMD suffers from a substantial decrease in water flux along the module. The exit water flux
637 decreased by 50% of the inlet value for DCMD, while it decreased by 2% for AGMD with 1mm
638 air gap thickness. Consequently, unlike the DCMD, it is not critical for AGMD to create a
639 uniform temperature distribution that minimise the decrease of water flux along the system.
640 Moreover, Re number which was relative to the inlet velocity and channel height, air-gap
641 thickness and module length determine the value of downstream variation of water flux in
642 AGMD.

643 Appendix

$$Nu = 4.36 + \frac{0.036RePr D_h/L}{1 + 0.0011(RePr D_h/L)^{0.8}} \quad [53, 54] \text{ (A1)}$$

$$Pr = \frac{c_p \mu}{k_{t,^\circ C}} \quad \text{(A2)}$$

$$h_{f,p} = \frac{Nuk_{f,K}}{d_h} \quad \text{(A3)}$$

$$Re = \frac{\rho u d_h}{\mu} \quad \text{(A4)}$$

$$\rho = 995.3 + 753.3c - 0.008442T^2 \quad [55] \text{ (A5)}$$

$$\mu = (2.367 + 2.205c - 0.491 \log T) \times 10^{-3}$$

$$c_p = (3.112 - 3.448c + T^{0.003406}) \times 10^3 \quad [55] \text{ (A6)}$$

$$k_{f,^\circ C} = 0.596 - 0.448c + 0.0006609T \quad [55] \text{ (A7)}$$

$$k_{f,K} = 0.5621 + 0.00199M + 0.000294MT - 2.3 * 10^{-6}MT^2 \quad [56] \text{ (A8)}$$

$$+ 0.00177M^2 - 6.3 * 10^{-5}TM^2 + 4.5 * 10^{-7}T^2M^2$$

$$\lambda_{a/w} = \frac{k_B T}{\pi [0.5(\sigma_w + \sigma_a)]^2 P_t} \cdot \frac{1}{\left[1 + \frac{M_w}{M_a}\right]^{0.5}} \quad [57] \text{ (A9)}$$

$$\begin{aligned}\sigma_a &= 3.711 \times 10^{-10} \\ \sigma_w &= 2.641 \times 10^{-10} \\ k_B &= 1.381 \times 10^{-23} \\ Kn &= \frac{\lambda_{a/w}}{d_p}\end{aligned}\quad [57] \text{ (A10)}$$

$$(J_w)_{ag} = \frac{(D_{v-a})_{ag}}{RT_{ag}b} \nabla P_{w|ag} + \frac{P_w}{P_t} ((J_w)_{ag} + (J_a)_{ag}) \quad (A11)$$

644 $(J_a)_{ag}$ is the influence of air flux, which moves counter to the water flux:

$$\frac{(J_a)_{ag}}{(J_w)_{ag}} = -\alpha_2 \quad (A12)$$

$$(J_w)_{ag} = -\frac{M_w}{RT_{ag}b} \left(\frac{P_t - (1 - \alpha_2)P_w}{(P_t D_{v-a})_{ag}} \right)^{-1} \nabla P_{w|ag} \quad (A13)$$

$$(J_w)_{ag,m,mu} = \frac{M_w(\epsilon/\tau)(P_t D_{v-a})_m (P_t D_{v-a})_{ag}}{R[\delta(1 - \alpha_1)T_m(P_t D_{v-a})_{ag} + b(\epsilon/\tau)(1 - \alpha_2)T_{ag}(P_t D_{v-a})_m]} \quad (A14)$$

$$\ln \left[\frac{T_m \delta(P_t D_{v-a})_{ag}(P_t - (1 - \alpha_1)P_{v,filim}) + T_{ag}b(P_t D_{v-a})_m(\epsilon/\tau)(P_t - (1 - \alpha_2)P_{v,filim})}{T_m \delta(P_t D_{v-a})_{ag}(P_t - (1 - \alpha_1)P_{v,filim}) + T_{ag}b(P_t D_{v-a})_m(\epsilon/\tau)(P_t - (1 - \alpha_2)P_{v,filim})} \right]$$

$$(J_w)_{ag,Kn} = \frac{M_w(P_t D_{v-a})_{ag}}{Rb(1 - \alpha_2)T_{ag}} \ln \left[\frac{D_{kn}T_{ag}b(P_t - (1 - \alpha_2)P_{v,filim}) + T_m \delta(P_t D_{v-a})_{ag}}{D_{kn}T_{ag}b(P_t - (1 - \alpha_2)P_{v,filim}) + T_m \delta(P_t D_{v-a})_{ag}} \right] \quad (A15)$$

$$D_{kn} = \frac{4\epsilon}{3\tau} d_p \sqrt{\frac{RT}{2\pi M_w}} \quad [42] \text{ (A16)}$$

$$P_t D_{wv-a} = 1.895T^{2.072} \times 10^{-5} \quad [58] \text{ (A17)}$$

$$\alpha_1 = \sqrt{\frac{M_w}{M_a}} \quad (A18)$$

$$P_w = a_w p_{sat} \quad [59] \text{ (A19)}$$

$$P_{sat} = \exp\left(23.5377 - \frac{4016.3632}{T - 38.6339}\right) \quad [59] \text{ (A20)}$$

$$a_w = 1 - 0.03112M - 0.001482M^2 \quad [59] \text{ (A21)}$$

645

646

647 Reference

648

- 649 1. Karagiannis, I.C. and P.G. Soldatos, *Water desalination cost literature: review and*
650 *assessment*. Desalination, 2008. **223**(1-3): p. 448-456.

- 651 2. Kumar, M., T. Culp, and Y. Shen. *Water Desalination: History, Advances, and*
652 *Challenges*. in *Frontiers of Engineering, Reports on Leading-Edge Engineering from*
653 *the 2016 Symposium*. 2017.
- 654 3. Ansari, A., et al., *An Improved Modelling Approach for the Comprehensive Study of*
655 *Direct Contact Membrane Distillation*. *Membranes*, 2021. **11**(5): p. 308.
- 656 4. Elcik, H., et al., *Multi-effect distillation brine treatment by membrane distillation:*
657 *Effect of antiscalant and antifoaming agents on membrane performance and scaling*
658 *control*. *Desalination*, 2020. **493**: p. 114653.
- 659 5. Xu, J., et al., *Effect of operating parameters and membrane characteristics on air gap*
660 *membrane distillation performance for the treatment of highly saline water*. *Journal*
661 *of Membrane Science*, 2016. **512**: p. 73-82.
- 662 6. Khalifa, A.E. and S.M. Alawad, *Air gap and water gap multistage membrane*
663 *distillation for water desalination*. *Desalination*, 2018. **437**: p. 175-183.
- 664 7. Ali, E., et al., *Integration of multi effect evaporation and membrane distillation*
665 *desalination processes for enhanced performance and recovery ratios*. *Desalination*,
666 2020. **493**: p. 114619.
- 667 8. Najib, A., et al., *Thermodynamics analysis of a direct contact membrane distillation*
668 *with/without heat recovery based on experimental data*. *Desalination*, 2019. **466**: p.
669 52-67.
- 670 9. Soukane, S., et al., *Scaling sets the limits of large scale membrane distillation*
671 *modules for the treatment of high salinity feeds*. *Journal of Cleaner Production*, 2021.
672 **287**: p. 125555.
- 673 10. Soukane, S., J.-G. Lee, and N. Ghaffour, *Direct contact membrane distillation module*
674 *scale-up calculations: Choosing between convective and conjugate approaches*.
675 *Separation and Purification Technology*, 2019. **209**: p. 279-292.
- 676 11. Soukane, S., et al., *Effect of feed flow pattern on the distribution of permeate fluxes*
677 *in desalination by direct contact membrane distillation*. *Desalination*, 2017. **418**: p.
678 43-59.
- 679 12. Noamani, S., et al., *Modeling of Air-Gap Membrane Distillation and Comparative*
680 *Study with Direct Contact Membrane Distillation*. *Industrial & Engineering Chemistry*
681 *Research*, 2020. **59**(50): p. 21930-21947.
- 682 13. Alsaadi, A.S., et al., *Evaluation of air gap membrane distillation process running*
683 *under sub-atmospheric conditions: Experimental and simulation studies*. *Journal of*
684 *Membrane Science*, 2015. **489**: p. 73-80.
- 685 14. Alsaadi, A.S., et al., *Modeling of air-gap membrane distillation process: A theoretical*
686 *and experimental study*. *Journal of membrane science*, 2013. **445**: p. 53-65.
- 687 15. Khayet, M. and C. Cojocar, *Air gap membrane distillation: Desalination, modeling*
688 *and optimization*. *Desalination*, 2012. **287**: p. 138-145.
- 689 16. Attia, H., et al., *Modelling of air gap membrane distillation and its application in*
690 *heavy metals removal*. *Desalination*, 2017. **424**: p. 27-36.
- 691 17. Hitsov, I., et al., *Full-scale validated Air Gap Membrane Distillation (AGMD) model*
692 *without calibration parameters*. *Journal of membrane science*, 2017. **533**: p. 309-
693 320.
- 694 18. Orfi, J., N. Loussif, and P.A. Davies, *Heat and mass transfer in membrane distillation*
695 *used for desalination with slip flow*. *Desalination*, 2016. **381**: p. 135-142.
- 696 19. Bindels, M., N. Brand, and B. Nelemans, *Modeling of semibatch air gap membrane*
697 *distillation*. *Desalination*, 2018. **430**: p. 98-106.

- 698 20. Alklaibi, A.M. and N. Lior, *Transport analysis of air-gap membrane distillation*.
699 Journal of membrane science, 2005. **255**(1-2): p. 239-253.
- 700 21. Karbasi, E., et al., *Experimental and numerical study of air-gap membrane distillation*
701 *(AGMD): novel AGMD module for Oxygen-18 stable isotope enrichment*. Chemical
702 Engineering Journal, 2017. **322**: p. 667-678.
- 703 22. Janajreh, I., et al., *Numerical investigation of air gap membrane distillation (AGMD):*
704 *Seeking optimal performance*. Desalination, 2017. **424**: p. 122-130.
- 705 23. Alpatova, A., et al., *Co-axial hollow fiber module for air gap membrane distillation*.
706 Journal of Membrane Science, 2019. **578**: p. 172-182.
- 707 24. Francis, L., et al., *Material gap membrane distillation: A new design for water vapor*
708 *flux enhancement*. Journal of membrane science, 2013. **448**: p. 240-247.
- 709 25. Duong, H.C., et al., *Evaluating energy consumption of air gap membrane distillation*
710 *for seawater desalination at pilot scale level*. Separation and Purification Technology,
711 2016. **166**: p. 55-62.
- 712 26. Alsaati, A. and A.M. Marconnet, *Energy efficient membrane distillation through*
713 *localized heating*. Desalination, 2018. **442**: p. 99-107.
- 714 27. Summers, E.K., *Experimental study of thermal performance in air gap membrane*
715 *distillation systems, including the direct solar heating of membranes*. Desalination,
716 2013. **330**: p. 100-111.
- 717 28. Chen, T.-C. and C.-D. Ho, *Immediate assisted solar direct contact membrane*
718 *distillation in saline water desalination*. Journal of Membrane Science, 2010. **358**(1):
719 p. 122-130.
- 720 29. Elhenawy, Y., et al., *Experimental and theoretical investigation of a new air gap*
721 *membrane distillation module with a corrugated feed channel*. Journal of Membrane
722 Science, 2020. **594**: p. 117461.
- 723 30. Khalifa, A., et al., *Experimental and theoretical investigation on water desalination*
724 *using air gap membrane distillation*. Desalination, 2015. **376**: p. 94-108.
- 725 31. Duong, H.C., et al., *Membrane scaling and prevention techniques during seawater*
726 *desalination by air gap membrane distillation*. Desalination, 2016. **397**: p. 92-100.
- 727 32. Sanmartino, J., et al., *Desalination and concentration of saline aqueous solutions up*
728 *to supersaturation by air gap membrane distillation and crystallization fouling*.
729 Desalination, 2016. **393**: p. 39-51.
- 730 33. Gryta, M., *Surface modification of polypropylene membrane by helium plasma*
731 *treatment for membrane distillation*. Journal of Membrane Science, 2021. **628**: p.
732 119265.
- 733 34. Gryta, M., *Mitigation of Membrane Wetting by Applying a Low Temperature*
734 *Membrane Distillation*. Membranes, 2020. **10**(7): p. 158.
- 735 35. Essalhi, M. and M. Khayet, *Application of a porous composite*
736 *hydrophobic/hydrophilic membrane in desalination by air gap and liquid gap*
737 *membrane distillation: a comparative study*. Separation and Purification Technology,
738 2014. **133**: p. 176-186.
- 739 36. Alkhudhiri, A., N. Darwish, and N. Hilal, *Treatment of saline solutions using air gap*
740 *membrane distillation: experimental study*. Desalination, 2013. **323**: p. 2-7.
- 741 37. Alkhudhiri, A. and N. Hilal, *Air gap membrane distillation: A detailed study of high*
742 *saline solution*. Desalination, 2017. **403**: p. 179-186.
- 743 38. Gryta, M., *Application of polypropylene membranes hydrophilized by plasma for*
744 *water desalination by membrane distillation*. Desalination, 2021. **515**: p. 115187.

- 745 39. Eykens, L., et al., *Direct contact and air gap membrane distillation: Differences and*
746 *similarities between lab and pilot scale*. *Desalination*, 2017. **422**: p. 91-100.
- 747 40. Eykens, L., et al., *How to select a membrane distillation configuration? Process*
748 *conditions and membrane influence unraveled*. *Desalination*, 2016. **399**: p. 105-115.
- 749 41. Incropera, F.P., et al., *Principles of heat and mass transfer*. 2013: Wiley.
- 750 42. Kast, W. and C.-R. Hohenthanner, *Mass transfer within the gas-phase of porous*
751 *media*. *International Journal of Heat and Mass Transfer*, 2000. **43**(5): p. 807-823.
- 752 43. Phattaranawik, J., R. Jiratananon, and A. Fane, *Effect of pore size distribution and*
753 *air flux on mass transport in direct contact membrane distillation*. *Journal of*
754 *Membrane Science*, 2003. **215**(1-2): p. 75-85.
- 755 44. Treybal, R.E., *Mass transfer operations*. New York, 1980. **466**.
- 756 45. Hirsch, C., *Numerical computation of internal and external flows: The fundamentals*
757 *of computational fluid dynamics*. 2007: Elsevier.
- 758 46. Fluent, A., *ANSYS Fluent Theory Guide, Release 18.0*. Ansys. 2017, Inc.
- 759 47. Fluent, A., ® *ANSYS [ANSYS Fluent], 15.0, Help System, User's Guide/Theory Guide*.
760 ANSYS, Inc., Canonsburg, PA, accessed Sept, 2017. **9**: p. 2019.
- 761 48. Khayet, M. and T. Matsuura, *Membrane distillation: principles and applications*.
762 2011.
- 763 49. Banat, F.A. and J. Simandl, *Desalination by Membrane Distillation: A Parametric*
764 *Study*. *Separation Science and Technology*, 1998. **33**(2): p. 201-226.
- 765 50. Vanneste, J., et al., *Novel thermal efficiency-based model for determination of*
766 *thermal conductivity of membrane distillation membranes*. *Journal of Membrane*
767 *Science*, 2018. **548**: p. 298-308.
- 768 51. Park, D.J., E. Norouzi, and C. Park, *Experimentally-validated computational*
769 *simulation of direct contact membrane distillation performance*. *International*
770 *Journal of Heat and Mass Transfer*, 2019. **129**: p. 1031-1042.
- 771 52. Chiam, C.-K. and R. Sarbatly, *Vacuum membrane distillation processes for aqueous*
772 *solution treatment—A review*. *Chemical Engineering and Processing: Process*
773 *Intensification*, 2013. **74**: p. 27-54.
- 774 53. Gryta, M. and M. Tomaszewska, *Heat transport in the membrane distillation process*.
775 *Journal of Membrane Science*, 1998. **144**(1): p. 211-222.
- 776 54. Khayet, M., *Membranes and theoretical modeling of membrane distillation: A review*.
777 *Advances in Colloid and Interface Science*, 2011. **164**(1): p. 56-88.
- 778 55. Carvalho, G., et al., *Physicothermal properties of aqueous sodium chloride solutions*.
779 *Journal of Food Process Engineering*, 2015. **38**(3): p. 234-242.
- 780 56. Ramires, M.L., et al., *Thermal conductivity of aqueous sodium chloride solutions*.
781 *Journal of Chemical and Engineering Data*, 1994. **39**(1): p. 186-190.
- 782 57. Johnson, R.A. and M.H. Nguyen, *Understanding membrane distillation and osmotic*
783 *distillation*. 2017: John Wiley & Sons.
- 784 58. Cussler, E.L. and E.L. Cussler, *Diffusion: mass transfer in fluid systems*. 2009:
785 Cambridge university press.
- 786 59. Hitsov, I., et al., *Modelling approaches in membrane distillation: A critical review*.
787 *Separation and Purification Technology*, 2015. **142**: p. 48-64.

788